Comptes Rendus

Chimie

Hester Colboc, Philippe Moguelet, Emmanuel Letavernier, Vincent Frochot, Jean-François Bernaudin, Raphaël Weil, Stéphan Rouzière, Patricia Senet, Claude Bachmeyer, Naomi Laporte, Ivan Lucas, Vincent Descamps, Reyhan Amode, Florence Brunet-Possenti, Nicolas Kluger, Lydia Deschamps, Arnaud Dubois, Solenn Reguer, Andrea Somogyi, Kadda Medjoubi, Matthieu Refregiers, Michel Daudon and Dominique Bazin

Pathologies related to abnormal deposits in dermatology: a physico-chemical approach

Microcrystalline pathologies: Clinical issues and nanochemistry / *Pathologies microcristallines : questions cliniques et nanochimie*

Pathologies related to abnormal deposits in dermatology: a physico-chemical approach

Hester Colboc [*, a], **Philippe Moguelet** [b], **Emmanuel Letavernier** [c, d], **Vincent Frochot** [c, d], **Jean-François Bernaudin** [e, f], **Raphaël Weil** [g], **Stéphan Rouzière** [g], **Patricia Senet** [h], **Claude Bachmeyer** [i], **Naomi Laporte** [a], **Ivan Lucas** [j], **Vincent Descamps** [k], **Reyhan Amode** [k], **Florence Brunet-Possenti** [k], **Nicolas Kluger** [k, l], **Lydia Deschamps** [m], **Arnaud Dubois** [n], **Solenn Reguer** [o], **Andrea Somogyi** [o], **Kadda Medjoubi** [o], **Matthieu Refregiers** [o], **Michel Daudon** [c, d] and **Dominique Bazin** [p]

[a] Sorbonne Université, AP-HP, Hôpital Rothschild, Service Plaies et Cicatrisation, Paris, France

[b] Sorbonne Université, AP-HP, Hôpital Tenon, Anatomie et Cytologie Pathologiques, Paris, France

[c] Sorbonne Université, AP-HP, Hôpital Tenon, Service d'explorations fonctionnelles, Paris, France

[d] INSERM, UMRS 1155, Sorbonne Université, Hôpital Tenon, Paris, France

[e] Faculté de médecine Sorbonne Université, Paris, France

[f] INSERM UMR 1272 Université Sorbonne Paris-Nord, Bobigny, France

[g] Université Paris-Saclay, CNRS, Laboratoire de Physique des Solides, 91405, Orsay, France

[h] Sorbonne Université, AP-HP, Hôpital Tenon, Service de Dermatologie, Paris, France

[i] Sorbonne Université, AP-HP, Hôpital Tenon, Service de Médecine Interne, Paris, France

[j] Sorbonne Université, UMR 8235, Paris, France

[k] Service de Dermatologie, AP-HP, Hôpital Bichat, Paris, France

[l] Department of Dermatology, Allergology and Venereology, Helsinki University Hospital, Helsinki, Finland

[m] Anatomie et Cytologie Pathologiques, AP-HP, Hôpital Bichat, Paris, France

[n] Laboratoire Charles Fabry, CNRS, Institut d'Optique Graduate School, Université Paris-Saclay, Palaiseau, France

[o] Synchrotron SOLEIL L'Orme des Merisiers Saint-Aubin, Synchrotron Soleil, Gif-sur-Yvette, France

[p] Université Paris-Saclay, CNRS, Institut de Chimie Physique, 91405, Orsay, France

* Corresponding author.

E-mails: hestercolboc@gmail.com (H. Colboc), philippe.moguelet@aphp.fr
(P. Moguelet), emmanuel.letavernier@aphp.fr (E. Letavernier),
vincent.frochot@aphp.fr (V. Frochot), jf.bernaudin-univ@orange.fr (J.-F. Bernaudin),
raphael.weil@u-psud.fr (R. Weil), stephan.rouziere@universite-paris-saclay.fr
(S. Rouzière), patricia.senet@aphp.fr (P. Senet), claude.bachmeyer@aphp.fr
(C. Bachmeyer), naomijylaporte@gmail.com (N. Laporte), ivan.lucas@upmc.fr
(I. Lucas), vincent.descamps@aphp.fr (V. Descamps), reyhan_amode@hotmail.com
(R. Amode), florence.brunet-possenti@aphp.fr (F. Brunet-Possenti),
nicolaskluger@yahoo.fr (N. Kluger), lydia.deschamps@aphp.fr (L. Deschamps),
arnaud.dubois@institutoptique.fr (A. Dubois), solenn.reguer@synchrotron-soleil.fr
(S. Reguer), andrea.somogyi@synchrotron-soleil.fr (A. Somogyi),
kadda.medjoubi@synchrotron-soleil.fr (K. Medjoubi),
matthieu.refregiers@synchrotron-soleil.fr (M. Refregiers),
daudonmichel24@gmail.com (M. Daudon),
dominique.bazin@universite-paris-saclay.fr (D. Bazin)

Abstract. Although numerous pathologies are associated with abnormal skin deposits, these remain poorly described, as accurate characterization continues to present a challenge for dermatologists. Their submicrometer size as well as their diverse chemistry require various characterization tools. We aim to exemplify characterization of endogenous and exogenous skin deposits in some selected skin diseases using different physico-chemical techniques. We begin with a presentation of selected diseases associated with skin deposits. We then present those of our results which show their variety of structure, location and chemical composition, obtained with various tools: Field Emission Scanning Electron Microscopy coupled with Energy Dispersive X-ray Spectroscopy, X-ray fluorescence, vibrational spectroscopies, as well as techniques specific to synchrotron radiation. Our results constitute a real opportunity to improve diagnosis, and to understand the pathogenesis of many skin diseases, and opportunities for therapeutic intervention.

Keywords. Dermatology, Calcification, Vibrational spectroscopies, Electronic microscopy, Synchrotron radiation.

Published online: 24 February 2022

1. Introduction

A wide variety of diseases produces pathological deposits in tissues, including cancers, genetic disorders, infectious processes and environmental diseases. Such diversity explains the strong interest of the scientific and the medical community in these pathological deposits, as well as the difficulty of establishing a meaningful relationship between their physicochemistry and the underlying pathology [1–6].

In dermatology, the medical literature reveals the same complexity, and various skin diseases are associated with either endogenous (mineral or organic) or exogenous deposits [7,8]. Mineral endogenous deposits are generally composed of calcium phosphate apatite deposits, and are often considered to be provoked by the skin disease itself [9], while exogenous deposits can present various chemical phases, and are often considered as potential disease causes [10].

Due to their submicrometer size as well as their chemical diversity, characterization of pathological deposits in the dermis cannot be performed with conventional techniques routinely used in hospital laboratories. Some standard staining procedures such as von Kossa, Yasu or alizarin red, can demonstrate the phospho-calcic nature of the deposits, but they do not provide further information on their chemical composition [11]. It is therefore necessary to develop physico-chemical techniques able to describe their structural characteristics at a micrometre, or even nanometer, scale, as well as their chemical composition [12,13]. Such an approach has been applied successfully to various pathological calcifications in different organs, such as the kidney [14,15], prostate [16,17] or thyroid [18,19].

Various techniques can be used, including Field Emission Scanning Electron Microscopy coupled with Energy Dispersive X-ray Spectroscopy (FE-SEM/EDX) [20–22], μX-ray fluorescence (XRF) [23–25], μX-ray scattering [26–29], vibrational spectroscopies: μFourier Transform Infra-Red (FTIR) and μRaman spectroscopies [30–35] as well as techniques

specific to synchrotron radiation [36–39] such as X-ray absorption near edge structure (XANES) [40–45]. These techniques allow the clinician a deeper understanding of the biophysical mechanisms related to the pathogenesis of an abnormal deposit [46], establish a medical diagnosis [47–50] and have a better idea of the effects of drugs on pathological calcifications [51].

The aim of this paper is to present structural and chemical characterisations of both endogenous and exogenous deposits seen in various skin diseases and to discuss the advantages and the limitations of different physico-chemical techniques.

2. Generalities regarding skin calcifications

We will first review definitions related to skin calcification with reference to the literature, after which we will present some recent results using physico-chemical techniques on various skin disease.

2.1. *Usual description of disease related to skin calcifications*

Skin calcification, also known as calcinosis cutis, has been described for decades, and linked to inflammatory, metabolic, tumoral, genetic and infectious skin diseases [52].

Various authors have proposed classifications of these diseases based on the physiological process leading to the pathological skin calcifications. Four categories are generally recognized: metastatic, dystrophic, idiopathic and iatrogenic calcifications [53], mainly distinguished based on their formation mechanism. The most commonly encountered skin calcifications are metastatic and dystrophic [52].

As Table 1 shows, skin calcifications are not always associated with abnormal calcium and phosphate serum levels. Dystrophic calcifications, for example, are induced by local tissue injury or abnormalities affecting collagen or elastic fibres specifically. Systemic sclerosis [54], lupus erythematosus [55], dermatomyositis [56], or mixed connective tissue diseases, are typical examples of skin pathologies that induce such tissue damage, leading to a calcification nidus. In contrast, metastatic calcifications result from skin calcifications that form on normal tissue adjacent to areas with abnormal calcium and/or phosphate metabolism [53].

Figure 1. Vascular (red arrow) and subcutaneous (green arrow) skin calcifications of the lower limb, in the case of chronic venous insufficiency and leg ulcers.

Some diseases are not easily classified into these categories. Pseudoxanthoma elasticum, for example, is an inherited disease, associated with both a deficit in anti-mineralizing factor (pyrophosphate) and alterations of elastic fibres [57]. The initial phenomenon causing the disease is still disputed, making calcifications observed in pseudoxanthoma elasticum difficult to classify from dystrophic to metastatic calcifications.

Many skin structures can be calcified, especially in the dermis, including vessel walls and dermal interstitium. Figure 1 illustrates the radiological aspects of dystrophic calcifications in chronic venous insufficiency and leg ulcers. Presence of both vascular calcifications, shown by the linear aspect of the deposit, and dermal calcifications, illustrated by a more scattered aspect, are depicted.

While in mammalian epidermis a characteristic calcium gradient exists between lower and up-

Table 1. Types of skin calcifications and related diseases with some of their mechanisms

Type of calcifications	Calcification mechanism	Related diseases
Metastatic	Systemic alteration of calcium phosphate metabolism	Chronic kidney disease Calciphylaxis Hyperparathyroidism Paraneoplastic syndrom Sarcoidosis

Dystrophic	Inflammation/cell death or mineral deposition at sites of tissue damage or alteration of collagen and elastin fibres
	Serum calcium and phosphate levels are within normal ranges
		Connective tissue diseases
		   Scleroderma
		   Lupus erythematosus
		   Dermatomyositis
		Cutaneous neoplasms
		Infection
		Trauma
		Chronic venous insufficiency
		Inherited disorders
		   Werner Syndrome
		   Pseudoxanthoma elasticum
		   Ehlers–Danlos syndrome
		   Familial tumoral calcinosis

Idiopathic	No underlying tissue damage or metabolic disorder	Subepidermal calcified nodules
Iatrogenic	Elevated tissue concentration of calcium and tissue damage at the site of extravasated calcium	Intravenous calcium or para-aminosalicylic acid

per layers of the epidermis, little data exists regarding the calcium gradient within the dermis [58–60]. A dermis calcium gradient and its disruption consequent on disease remodelling of skin structures may play a role in skin calcification. However, not all patients with disrupted calcium-phosphate metabolism, nor all patients with local tissue injury, develop skin calcifications. It is probably the consequence of a complex interaction between metabolic disorders and genetic predispositions.

2.2. *Diversity of skin calcification localisation and morphology*

Latest generation FE-SEM allows a submicrometer scale structural description of these calcified deposits [20–22]. While optical microscopy is limited to a magnification of ca. 1000 (i.e. with a 100× objective and a 10× eyepiece), low voltage electrons can define skin surface topology at magnifications greater than

10,000, constituting a unique opportunity to describe micro calcifications undetected optically.

For our observations, we used a Zeiss SUPRA55-VP SEM, a field-emission "gun" microscope (FE-SEM) operating at 0.5–30 kV. High-resolution observations were obtained using an Everhart-Thornley SE detector. An in-lens SE detector is also available. All the measurements were taken at low voltage (between 0.5 and 2 kV) without the usual carbon deposits at the sample surface. Electron induced X-ray fluorescence experiments are also possible. Five micron tissue slices were deposited on low-e microscope slides (MirrIR, Kevley Technologies, Tienta Sciences, Indianapolis) to enable IR measurements to be performed on the very same sample [13]. Figure 2 shows five skin slices deposited on the low-e microscope slide and positioned in the FE-SEM.

Based on such FE-SEM observations, we identified three different locations where skin calcifications are typically observed: hypodermis, vessel, and der-
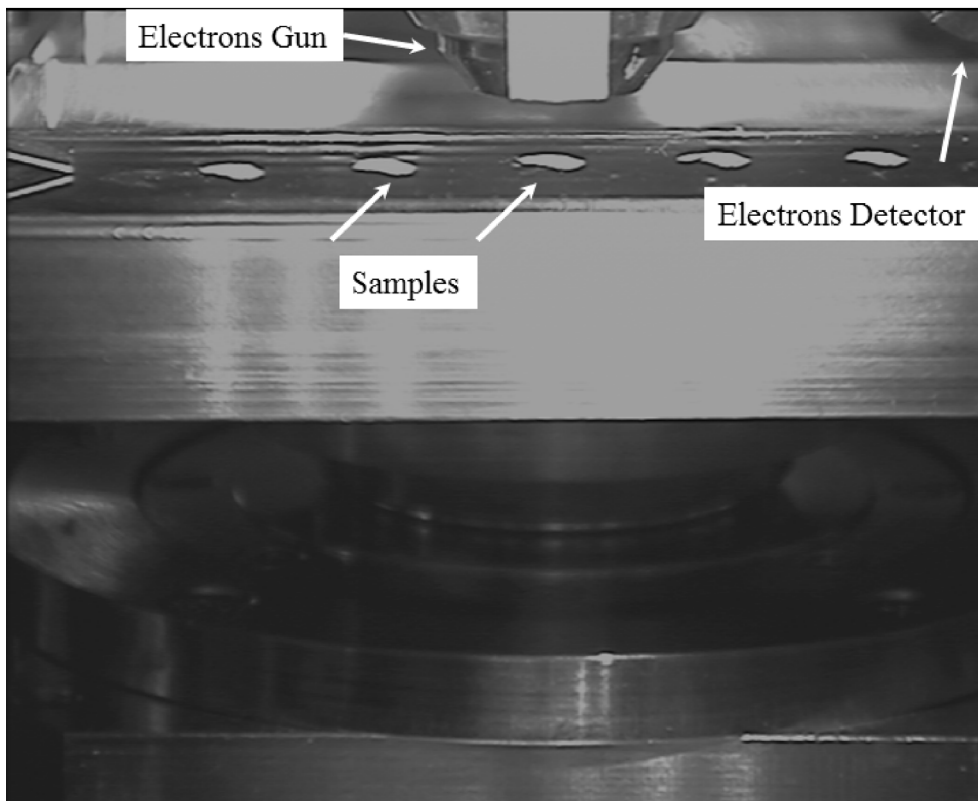
Figure 2. Skin biopsy slices are shown on the low-e microscope slide, positioned in the FE-SEM.

mal fibres (Figure 3). These micrometer scale descriptions constitute a significantly complementary approach to the usual routine hospital radiologic observations shown in Figure 1. Indeed, the spatial resolution of radiological measurements is far inferior [61]; FE-SEM therefore provides unique information regarding the exact location of sub micrometer pathological skin deposits.

FE-SEM also provides information on the morphology of the pathological calcifications. Morphology of skin calcifications varies: in Figure 3A and B calcifications appear as voluminous plaques while on Figures 3C, 4 and 5, high magnification emphasizes sub-micrometre spherical entities.

Calcification size is also very variable. Some are nanometric, making them difficult to identify. For example, in Figure 5 we can see that the calcification size is less than 1 μm.

Regarding the formation mechanisms of the different morphologies of skin calcification, we can hy-

pothesize that the agglomeration of small spherical bodies leads to the formation of a plaque (Figure 6A). A similar mechanism has been identified in ectopic breast calcifications [62] (Figure 6B). These similarities hightlight the fact that the pathogenesis of ectopic calcifications can be similar although the tissue and its function may be very different.

2.3. *Chemical diversity of skin calcifications*

Literature regarding the chemical composition of skin calcifications is scanty. What exists almost consistently reports carbapatite (calcium phosphate apatite) [63–65] as a unique chemical phase in the skin, which was usually the case in the samples we studied. However, our complete set of investigations reveals at least three chemical phases: namely calcite (one of the $CaCO_3$ polymorphs [66]), amorphous carbonated calcium phosphate (ACCP) and carbapatite (Table 2). More precisely, in both calciphylaxis and arte-
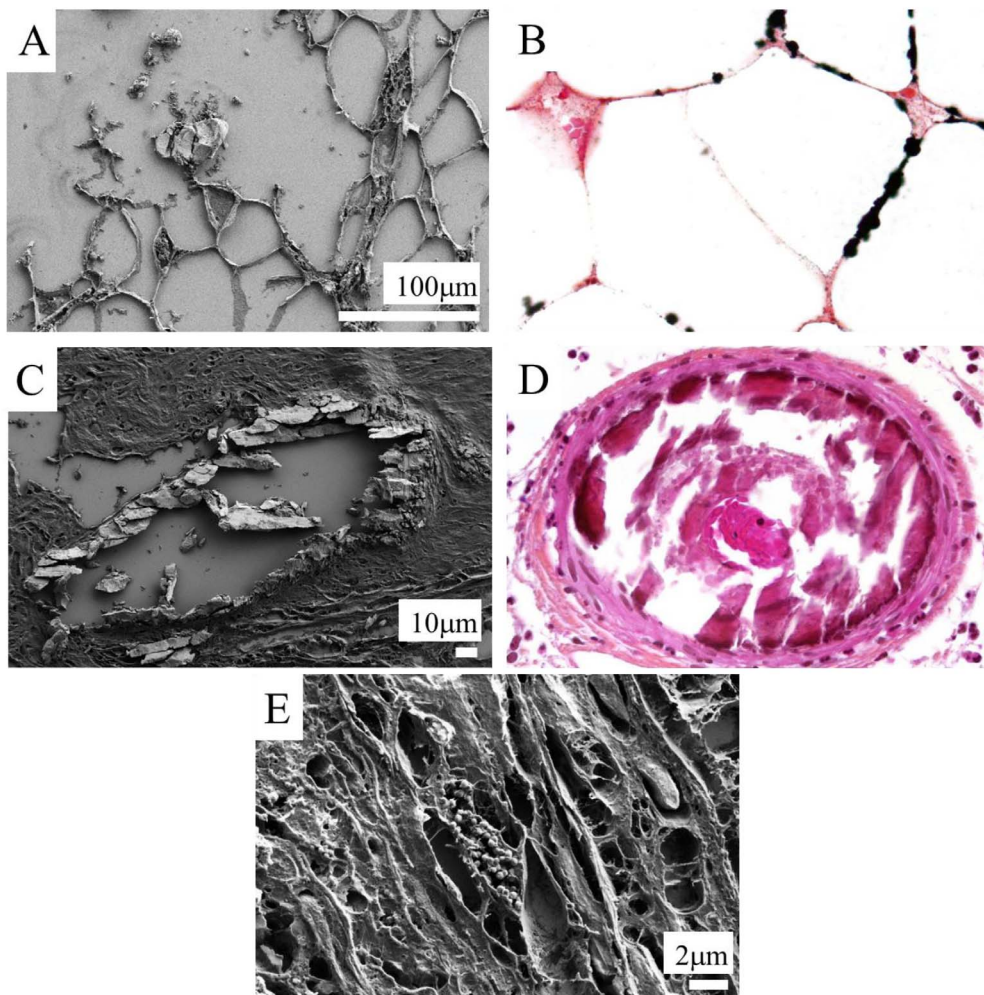
Figure 3. Different skin calcification localisation. Calcification in the hypodermis in cases of calciphylaxis; (A) FE-SEM, (B) Von Kossa-stained ×400. Massive circumferential calcifications of a dermal capillary in cases of calciphylaxis; (C) FE-SEM, (D) HES-stained ×400. (E) Nanometric spherical calcifications in dermal fibers in a case of sarcoidosis, not visible in optical miscroscopy. FE-SEM.

riosclerosis, we identified carbapatite, while calcium deposits observed in sarcoidosis were composed of calcite. The variety of dermal fibre structural modification associated with different skin diseases may lead to different modifications of skin functions and therefore the formation of different chemical types of calcifications.

Very few studies discuss the chemical diversity of skin calcifications. Among these, a report by Reid and Andersen [67] mentioned the presence of dolomite (not really a true calcium carbonate as its stoichio-

metric formula is $CaMg(CO_3)_2$). Yet, this chemical diversity has been well described in other organs: different calcium carbonate polymorphs have been identified in pancreatic stones, gallstones, salivary stones, and in the liver [68–71]. A better understanding of the chemical variety of skin calcifications would probably help in understanding the pathophysiology of these skin diseases, as well as the therapeutic options.

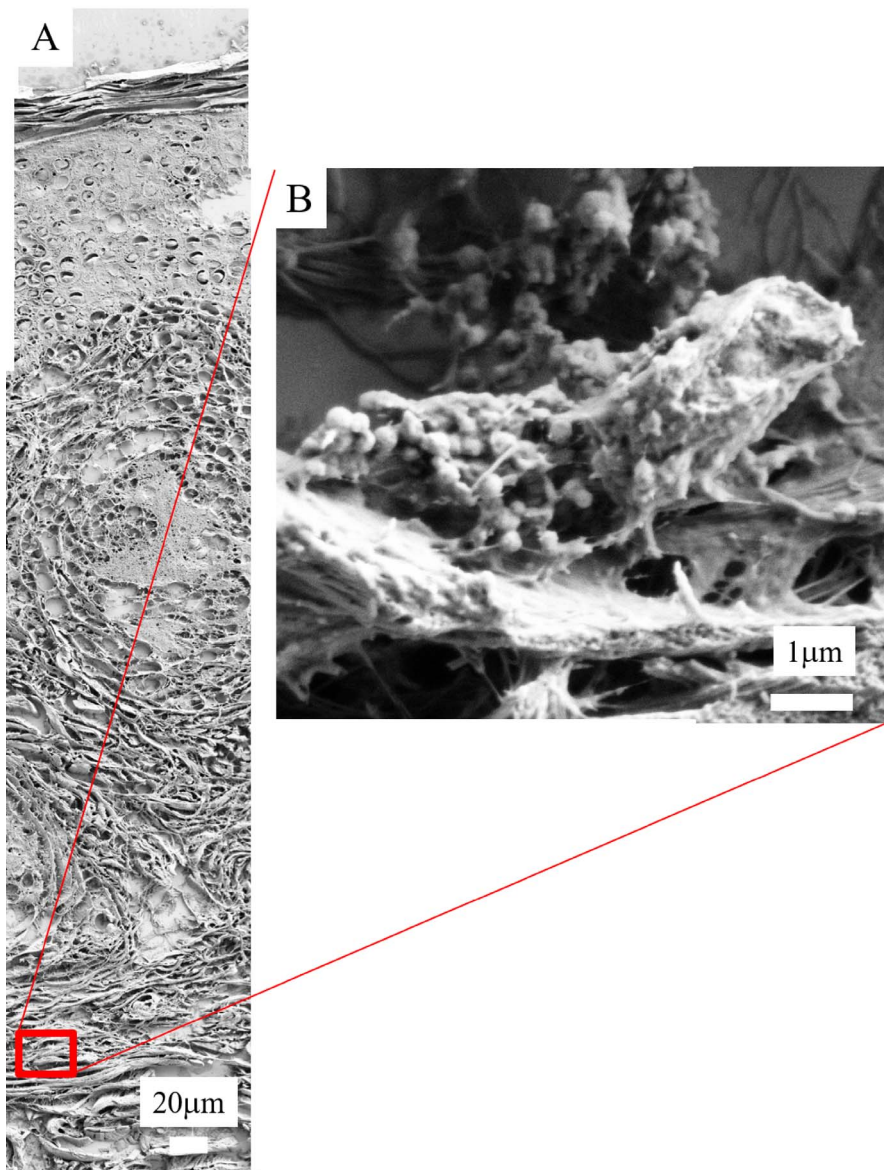Carbapatite and its precursor ACCP represent compounds identified in pathological calcifica-

Figure 4. Calcified spherical bodies at the periphery of a granuloma in a sarcoidosis case, observed using FE-SEM.

tions present in kidney, cartilage, thyroid, aortic valve, and breast [72–76]. At this point, it would be useful to summarize some relevant chemical characteristics of carbapatite. Biological apatites correspond to substituted calcium hydroxyapatite (HAP, $Ca_{10}(PO_4)_6(OH)$) [77–81]. The fundamental structure can tolerate substitutions by other ions with the same or a different charge. Some cations which

can replace Ca^{2+} are Pb^{2+}, Sr^{2+}, Co^{2+}, Zn^{2+}, Fe^{2+}, Cu^{2+} or Mg^{2+}. Investigations regarding a possible insertion of these cations in biological apatite have thus been performed [82–84]. Other substitutions involve replacement of the original PO_4^{3-} and OH^- anions which may have the same or a different electric charge (for example F^- substituted for OH^- or CO_3^{2-} substituted for PO_4^{3-} and/or OH^-). This wide range of
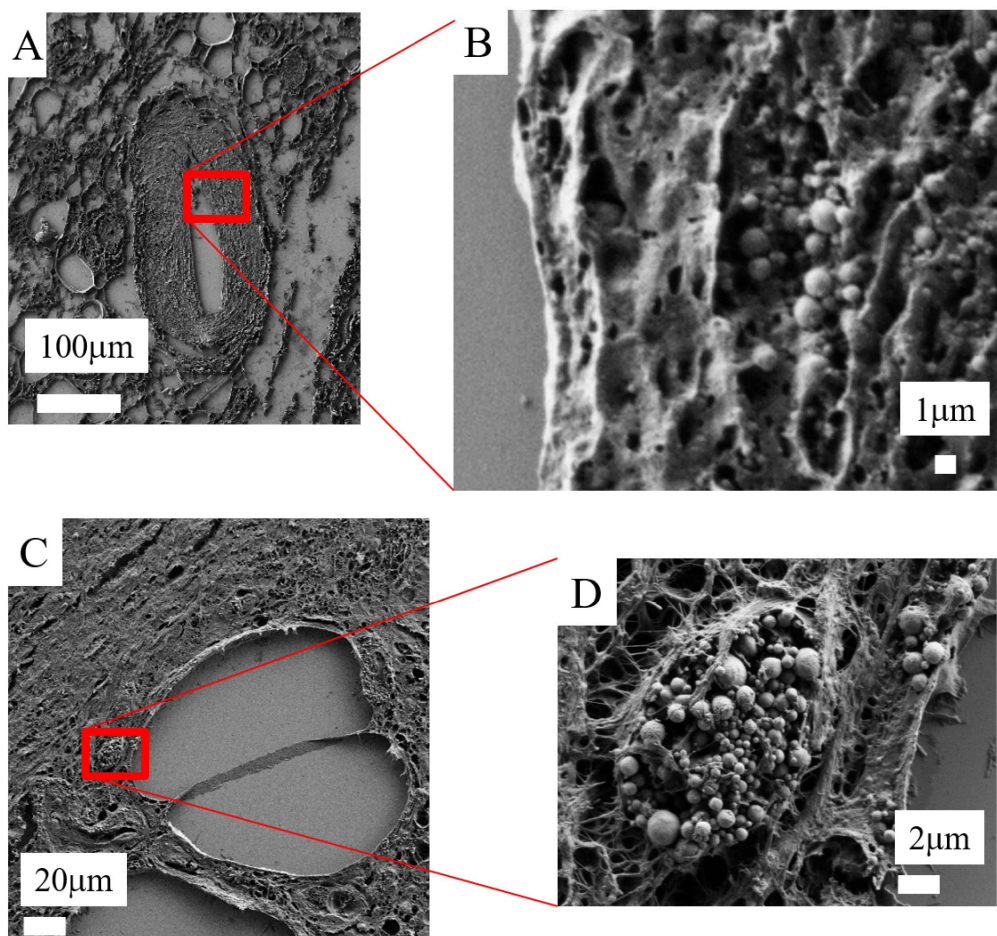
Figure 5. Calcified spherical bodies in a case of calciphylaxis, observed using FE-SEM in the vessel wall (A and B) and on the surface of an adipocyte (C and D).

ion substitutions can modify the physico-chemical and biological properties of apatites.

Numerous studies have been devoted to apatites which are conventionally regarded as conforming to the $A_5(BO_4)_3X$ canonical chemical formula [85,86]. The crystallographic structure (Figure 7) of apatite is well known, the space group is $P6_3/m$ with $a = b = 9.41844$ Å, $c = 6.88374$ Å [87,88].

The framework of the stoichiometric calcium hydroxyapatite can be described as an assemblage of tetrahedral PO_4 groups [89,90]. An interesting aspect of this is the existence of two channels. The first has a diameter of 2.5 Å and is surrounded by Ca^{2+} cations while the second is wider (3–4.5 Å).

Finally, biological apatites display some specific features. One is the widely reported deficiency of OH$^-$ [91–93]. Another, established more recently, is the presence of hydrogen phosphate (HPO_4^{2-}) ions in PO_4^{3-} sites [94]. Thus, as proposed by Combes *et al.* [80], we report in Table 2 the general formulae for biological apatites.

Regarding physicochemical investigations of biological apatites, it is of major importance to underline that the physicochemical characteristics of calcium phosphate apatite may significantly influence medical diagnostic. For example, in kidney stones, a high carbonate level in calcium phosphate apatite, as well as the presence of amorphous calcium phosphate apatite, indicate an infectious process implying the need for antibiotics [48,95]. The morphology of the kidney stones at the macroscopic scale as well as the morphology of calcium phosphate apatite
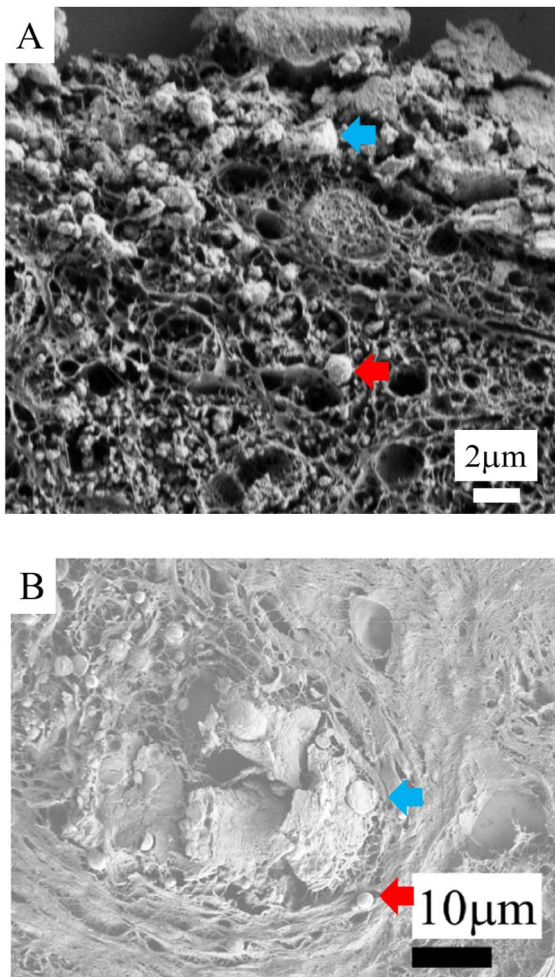
Figure 6. FE-SEM: (A) Agglomeration of spherical bodies (red arrow) leading to the formation of a plaque (blue arrow) in a case of calciphylaxis. (B) Comparison with calcification in a case of breast cancer: agglomeration of spherical bodies (red arrow) leading to the formation of a plaque (blue arrow).

crystallites at the micrometre scale may indicate an inherited distal renal tubular acidosis [49] or primary hyperoxaluria [47,96]. Finally, its zinc content may indicate inflammatory processes [84,97,98].

Another interesting aspect is that calcification morphology at the micrometre scale is not predictive of its chemistry. Spherical calcifications, for example, could be composed of either calcite or carbapatite. The calcification localisation (vascular, dermal or hypodermal) within the skin tissue again does not correlate with chemical composition, suggesting a relatively modest contribution of the skin tissue environment to the calcifications chemistry.

3. Generalities regarding exogenous skin deposits

The exposome concept was conceived in 2005 to represent the environmental, i.e. non-genetic, drivers of health and disease [99]. The exposome concept takes into account exposure to particles present in food and air or directly in contact with the skin. Skin protects the body from the external environment and it is therefore directly impacted by the exposome.

Penetration of this exogenous material can occur after a trauma, an injection, or a tattoo puncture; they have also been shown to penetrate into the skin through follicular orifices, for example after cosmetic application [100].

There is an increasing interest in understanding the effects of exogenous materials, including nanoparticles, on living tissues, among them skin. Recent developments in nanotechnology have established a link between exogenous deposits and some inflammatory diseases, such as in sarcoidosis [101, 102], frontal fibrosing alopecia [103,104] and tattoos [105,106].

4. Physico-chemical characteristics of deposits in various skin diseases

4.1. *Calciphylaxis*

Calciphylaxis is a disease with high morbidity. It affects up to 4% of patients with end stage renal disease, and its incidence rate increases for those on chronic hemodialysis [107]. Calciphylaxis is unlikely for patients with normal renal function.

The significant morbidity and mortality of calciphylaxis results from extensive skin necrosis, septic complications, and organ failure, which are the direct consequences of these ectopic calcifications. Female sex, diabetes mellitus, high body mass index, elevated calcium, phosphorus, and parathyroid hormone serum levels, nutritional status, and cinacalcet or vitamin K antagonist treatments, are associated with an increased risk of developing the disease [108,109].
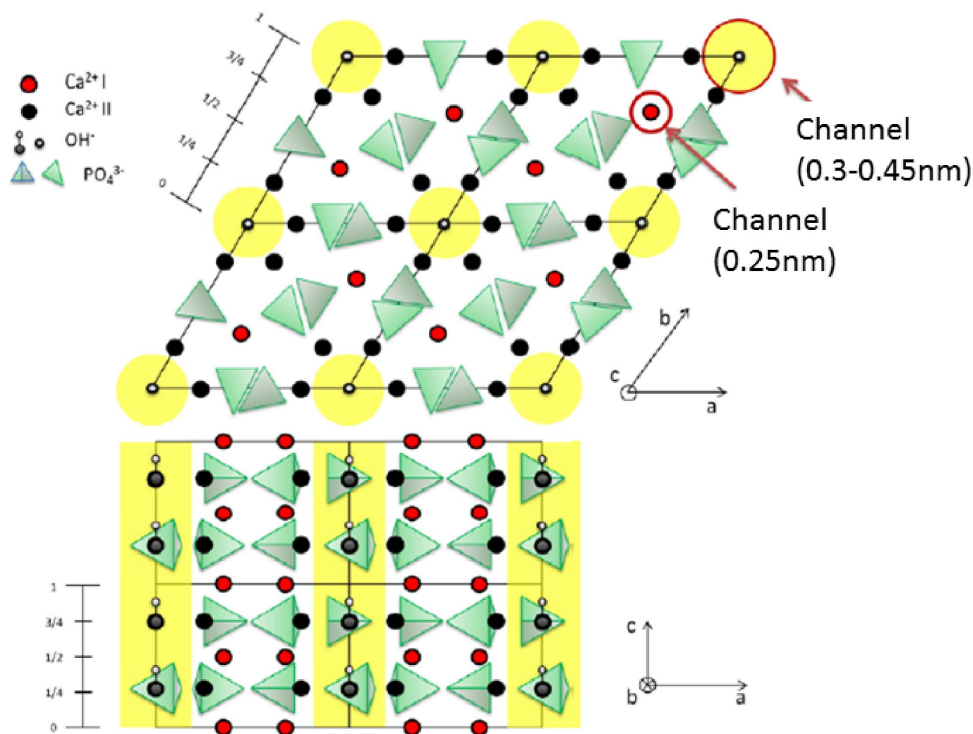
Figure 7. Crystallographic structure of the apatite 001 (top) and 010 (bottom) planes (from Ref. [77]).

Table 2. Different calcium phosphate compounds with their stoichiometry and their Ca/P ratio

Skin diseases	Serum calcium and phosphate levels	Calcifications' localisation	Chemical phase	Stoichiometry
Calciphylaxis	Usually elevated	Vessels, dermis, hypodermis	Amorphous carbonated calcium phosphate (ACCP)	$Ca_9(PO_4)_6\, nH_2O$
Calciphylaxis	Usually elevated	Vessels, dermis, hypodermis	Carbapatite	$Ca_{10-x}(PO_4)_{6-x}(HPO_4^{2-}$ or $CO_3^{2-})_x(OH)_{2-x}$ with $0 \leq x \leq 2$
Sarcoidosis	Usually normal	Dermis (surrounding granulomas)	Calcite	$CaCO_3$

Treatments usually achieve poor outcomes. They include calcimimetics, surgical parathyroidectomy, sodium thiosulfate, and bisphosphonates [110–112]. Pathogenesis of the disease is still under debate. Calcifications observed in calciphylaxis are considered to be metastatic calcifications, as they occur in patients with a phospho-calcic metabolic disturbance [52,53]. However, some authors also suspect that metalloproteinase digestion of elastin might occur in calciphylaxis, enhancing deposition of calcium within these modified elastic fibres [113]. In this hypothesis, calcium deposits in calciphylaxis could also be considered as dystrophic calcifications. Other authors suspect that metal deposits in the skin tissue are a trigger for a phenotypic switch of vascular smooth muscle cells from a contractile to an osteogenic phenotype [114].

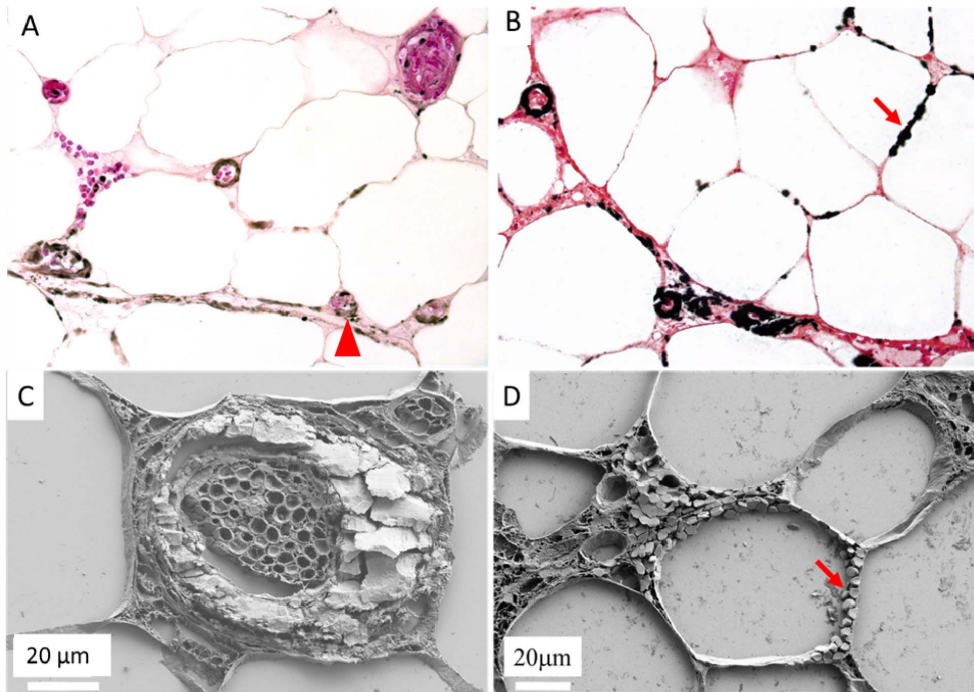Recently, we have combined FE-SEM observa-

Figure 8. Optical microscopy and FE-SEM comparisons in calciphylaxis. Optical microscopy showing multiple calcifications along adipocytes and in vessels walls, (A) Hypodermis, arrow head: calcified vessel, HES ×400, (B) Hypodermis, arrow: calcifications along adipocytes, Von Kossa ×400. FE-SEM: (C) Massively calcified vessel, (D) Calcifications along adipocytes.

tions of calcic skin deposits in calciphylaxis with FT-IR and Raman spectroscopic chemical analysis, and compared these results to calcifications observed in arteriosclerosis [63]. We showed that calcifications in calciphylaxis are composed of carbapatite, always located circumferentially, mostly in the intima of otherwise normal-looking vessels and often associated with interstitial deposits (Figure 8). Although vascular calcifications in arteriosclerosis were also composed of carbapatite, they are associated with medial hypertrophia, localized to parts of the vessel, and not associated with interstitial deposits. These results suggest a different pathogenesis and provide new insights into calciphylaxis pathogenesis that could explain the poor outcomes of vasodilators compared with the relative effectiveness of calcium-solubilising-drugs.

4.2. *Sarcoidosis: cases of exogeneous and endogenous abnormal deposits*

Sarcoidosis or Besnier–Boeck–Schaumann disease [115] is a chronic, multiorgan inflammatory disorder. The disease onset peaks during the third and fourth decades of life, and has a higher incidence among women and in Afro-American patients [116,117]. If the lungs are affected, in the vast majority of diagnosed patients other organ systems are often affected as well [118,119]. According to literature [120], skin is the second most affected organ, and may be involved in 25% to 30% of cases. Cutaneous sarcoidosis preferentially affects sites of prior injury such as tattoos [121,122] and scars [123].

Although clinical phenotypes, particularly of cutaneous lesions, are widely variable, the hallmarks of sarcoidosis are always noncaseating epithelioid and giant cell granulomas. The granulomatous inflammation (Figure 9) observed in sarcoidosis is considered to be caused by a complex interaction between
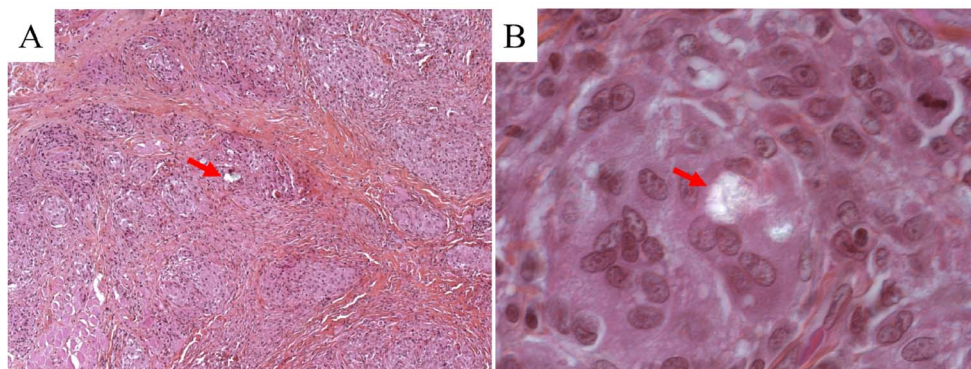
Figure 9. Optical microscopy and polarized light examination of granulomas in skin sarcoidosis, showing birefringent particles (arrow): (A) HES ×100, (B) HES ×400.

genetic background, environmental agents, infectious antigens, and T lymphocyte driven immune reactions [124].

Sarcoidosis, as well as being observed in other granulomatous diseases, is associated with calcium metabolism disorders. High serum calcium levels are seen in 5 to 10% of patients, mainly due to dysregulated production of calcitriol by activated macrophages which form the granulomatous lesions. These metabolic disturbances may lead to calcium deposits in various organs, including the skin, causing metastatic calcifications [125]. Reid and Andersen have indeed reported the presence of calcium oxalate and phosphate deposits in sarcoidosis involving lymph nodes and lungs [67]. Even though these chemical analyses have been done in different organs, they have never been performed in skin sarcoidosis.

Exact causes of the disease are still unknown; however the role of environmental mineral particles is highly suspected on epidemiological grounds [126]. There is a polarizable material in the centre of some granulomas, suggesting that foreign materials could be a nidus for granuloma formation and a potential trigger for the disease [127–130]. Using biopsy specimens of granulomatous lesions from 50 patients, Kim *et al.* [131] have estimated the frequency of polarizable foreign bodies in cutaneous lesions of sarcoidosis. These authors noticed that polarizable foreign bodies were present in the granulomatous skin lesions of 12 of 50 patients (24%) with cutaneous sarcoidosis. Using electron probe microanalysis, they identified the following elements: Calcium, phos-

phorus, silicon, and aluminium. Unfortunately, such a characterization technique is not able to identify the compounds in which these elements occur.

Electron microscopy has been used in several previous investigations [114–118]. For example, Takemura *et al.* [132] clearly demonstrated that ultrastructural examination improves the diagnostic utility of endomyocardial biopsy in cardiac sarcoidosis, by clearly identifying even only one epithelioid cell. More recently, Kuribayashi *et al.* [133] showed by electron microscopy that multinuclear giant cells were formed by epithelioid histiocytes and an aggregation of lymphocytes. Interesting FE-SEM results by Catinon *et al.* [134] indicate the presence of calcium phosphate particles in 7 out of 10 patients.

Recently, we have investigated 14 skin biopsies from cutaneous sarcoidosis patients by FE-SEM/EDX and FTIR spectroscopy [135,136]. FE-SEM allowed the identification in three patients of silica in the centre of skin granulomas (Figure 10). Some FE-SEM apparatus are able to acquire X-ray fluorescence spectra [20–22] so it is possible to know the elementary composition of specific materials in the tissue. Note that this selection can be performed at the submicrometer scale when electrons are employed as probes.

Figure 10E displays the X-ray fluorescence spectra induced by the primary electrons of the microscope on the foreign material we identified, and we can clearly see the contributions of Si ($K_\alpha = 1.740$ keV) and the contributions of other elements in the support (Zn, $L_{\alpha 1} = 1011.7$ keV; Ag, $L_{\alpha 1} = 2.984$ keV).
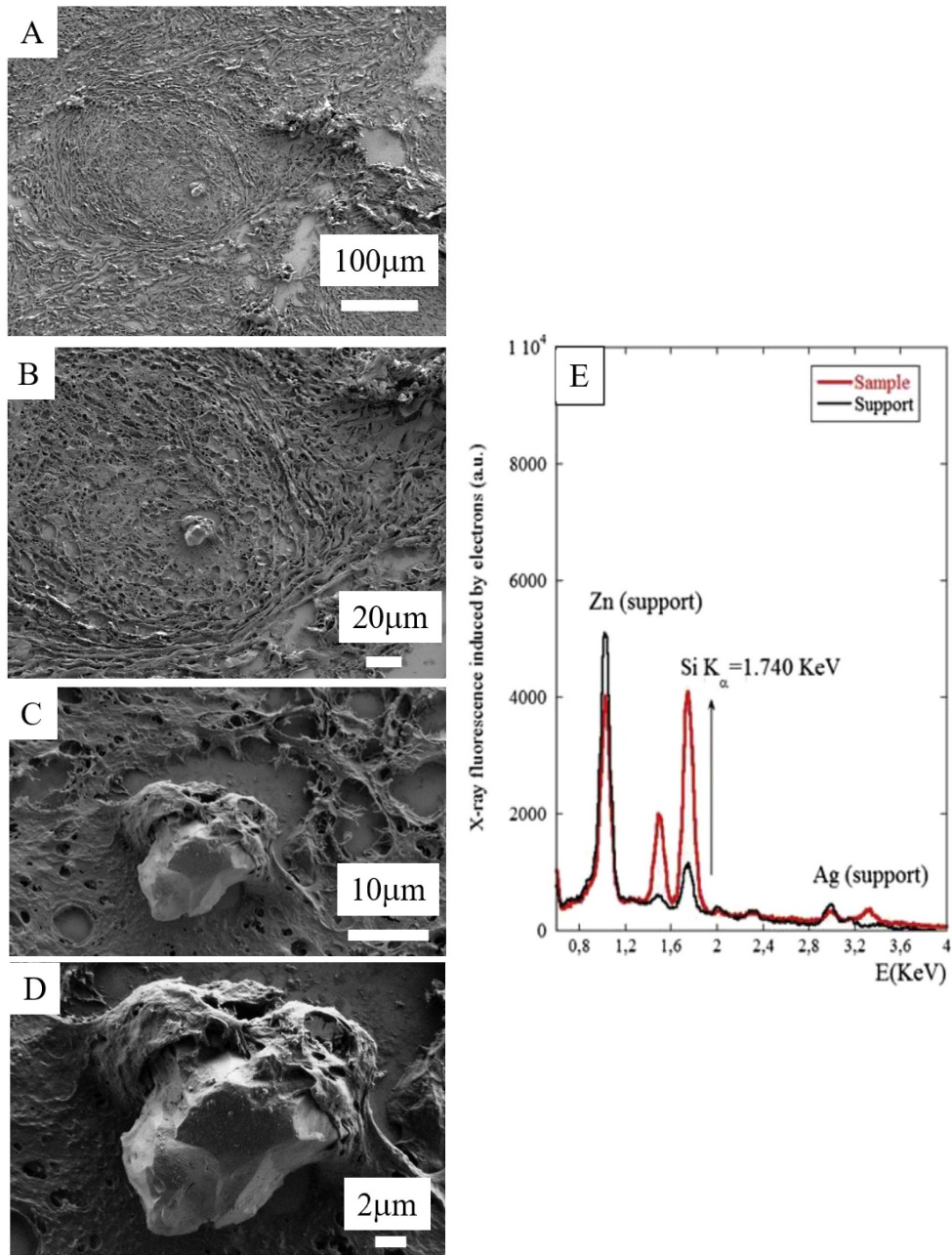
Figure 10. (A–D) FE-SEM photographs of foreign material in the skin biopsy of the arm of a patient with cutaneous sarcoidosis. (E) EDX spectrum identifies silica in the abnormal deposit at the centre of the granuloma.

To determine the chemical nature of the foreign material precisely, FTIR data have been collected on the same sample. Infrared spectroscopy is an advantageous, non-destructive, and label-free tech-nique for chemical analysis of biological tissues (Figure 11) [137–139]. This spectroscopy detects vibra-tional energy levels and phonons of materials and leads to precise chemical and structural information
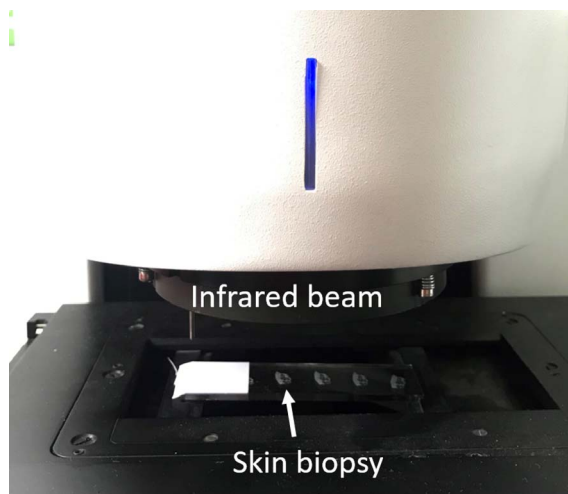
Figure 11. Slices from a skin biopsy are visible on the low-e microscope slide, which is positioned in the FTIR spectrometer.

by comparison with data bank reference spectra [30].

It is convenient to conceptualize an IR spectrum as two regions: 4000–1000 cm^{-1} known as the functional group region, and <1000 cm^{-1} known as the fingerprint region, even if for many chemists the dividing line is in fact 1450 cm^{-1}. The functional group region contains relatively few peaks, which are typically associated with the stretching vibrations of functional groups. In the fingerprint region, the spectra usually consist of bending vibrations within the molecule. This region is the key to the data analysis because it is here that each distinct compound produces its own unique pattern of peaks, effectively a fingerprint [140–143].

A large number of investigations are based on another vibrational spectroscopy, namely Raman [33–35]. As emphasized by Khulbe and Matsuura [144, 145], infrared and Raman spectra of a given molecule complement each other. The symmetrical stretching, n1 (normal vibration) of CO_2 is infrared inactive, but active in Raman. On the contrary, the bending, v_2, and asymmetric stretching, v_3, vibrations are Raman inactive and infrared active.

These differences arise from the fact that infrared spectroscopy exploits an absorption process dependent on the permanent dipolar moment of a molecular bond, while Raman spectroscopy is a scattering process related to a modification of the polarizability (induced change of the dipolar moment) of the molecule.

Recently, Krafft *et al.* [146] have compared these two spectroscopies in colon tissue applications. These authors note that the advantages of FTIR imaging are related to shorter acquisition times and higher spectral quality, while Raman imaging displays better spatial and spectral resolution. Also, significant differences also exist with respect to the preparation of biological tissue samples.

In Figure 12, the infrared bands show clearly that the foreign material is composed of crystalline silica [135], a chemical characteristic clearly indicating an exogenous origin of this abnormal deposit.

As we have seen previously, FE-SEM also offers the possibility of precisely describing skin deposits. For two of the samples, we have been able to pinpoint nanometer scale spherical bodies between the collagen fibres not detectable by classical optical microscopy. To determine their chemical composition (Figure 13A), we performed FTIR spectroscopy (Figure 13B) as well as EDX measurements (Figure 13C). Based on specific IR absorption bands, we can conclude that the spherical entities are calcite. On EDX analysis, we noticed the absence of a fluorescent P signal (2.01 keV) and the presence of a significant signal related to Ca (3.7 keV) in line with the FTIR spectrum showing the presence of calcite.

Another striking result of this investigation was the identification of spherical calcite entities in the periphery of the granuloma in 4 patients. This is in line with the fact that sarcoidosis, as well as observed
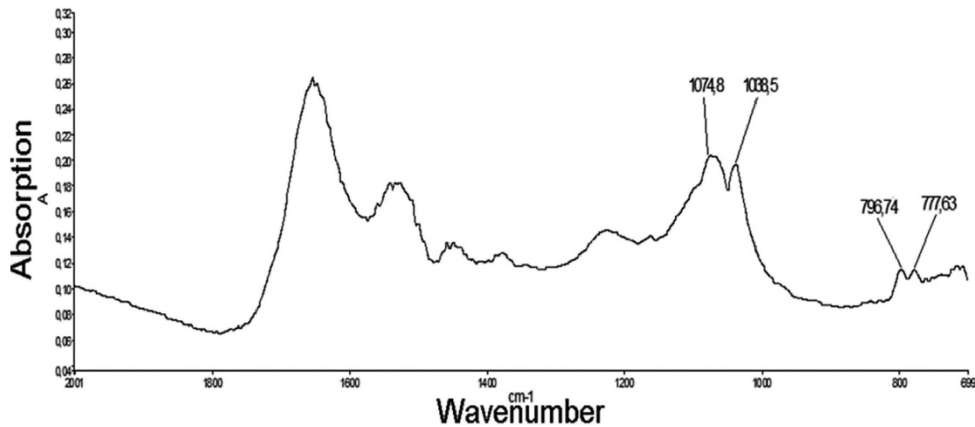
Figure 12. Infrared spectrum of the foreign material. The absorption bands at 1074 and 1038 cm^{-1} are associated with crystalline silica. Also, we can clearly see the α-quartz doublet (Silica) around 800 cm^{-1} in accordance with established infrared spectrometric data [30].

in other granulomatous diseases, is associated with calcium metabolism disorders [146,147].

Based on the entirety of our data, sarcoidosis exemplifies a case where both endogenous and an exogenous pathological deposit can be identified. Note that the presence of the nanometer scale endogenous calcifications cannot be discerned through classic staining procedures. This specific chemical composition observed only in sarcoidosis may be due to the significant dermal structure modification observed in the disease, which modifies the physiological spatial distribution of calcium through granuloma driven skin restructuring. A well-developed sarcoid granuloma consists of a tightly packed conglomerate of epithelioid- and multinucleated-giant cells encircled by lymphocytes, especially CD4+ T helper cells, but also rare CD8+ T cells and B cells [147–149]. Such reorganisation may lead to a specific calcification pathogenesis in sarcoidosis, explaining the presence of calcite and not carbapatite.

4.3. *Tattoo-associated keratoacanthoma*

Tattooing involves introducing pigmented material into the dermis by puncturing the skin, in order to obtain a permanent design. It is a very old practice, which has probably been performed since the Neolithic times [150]. Nowadays, tattoos are very widespread: in Europe, there are around 100 million people with tattoos [151,152]. Tattoo inks are made of almost insoluble pigments mixed with additives such as formulants, dispersants, and preservatives [153, 154]. Nowadays, natural pigments are very rarely used, and most tattoo inks are composed of synthetic substances [155–160], allowing cheaper mass production of inks with a large variety of shades. The composition of tattoo inks is poorly regulated worldwide, including in Europe, with few recent guidelines [161,162]. Various types of carcinogenic compounds occur in tattoo inks, including primary aromatic amines (PAA), cleavage products of organic azo colourants used in the inks [163]. Tattoos therefore effectively present permanent lifelong exposure to potentially carcinogenic compounds [164,165]. Many cases of skin cancers occurring within tattoos have been reported, including cases of keratoacanthoma (KA) on red ink, and the role of PAA is suspected [166,167]. Furthermore, cases of multiple or recurrent KA on tattoos have been reported, making the causality link between these skin tumours and tattoos even stronger [168].

Recently, we published an investigation regarding the chemical composition and distribution of tattoo inks within tattoo associated KA [169]. Clinical and histopathological data from three patients coming from Bichat Hospital diagnosed with tattoo associated KA in 2017 were selected (Figure 14). The medical file was completed by structural and chemical characterisation of tattoo inks within KA.

Regarding laboratory characterization techniques, we used X-ray fluorescence (XRF) [23–25] to identify the inorganic elements and Raman spec-
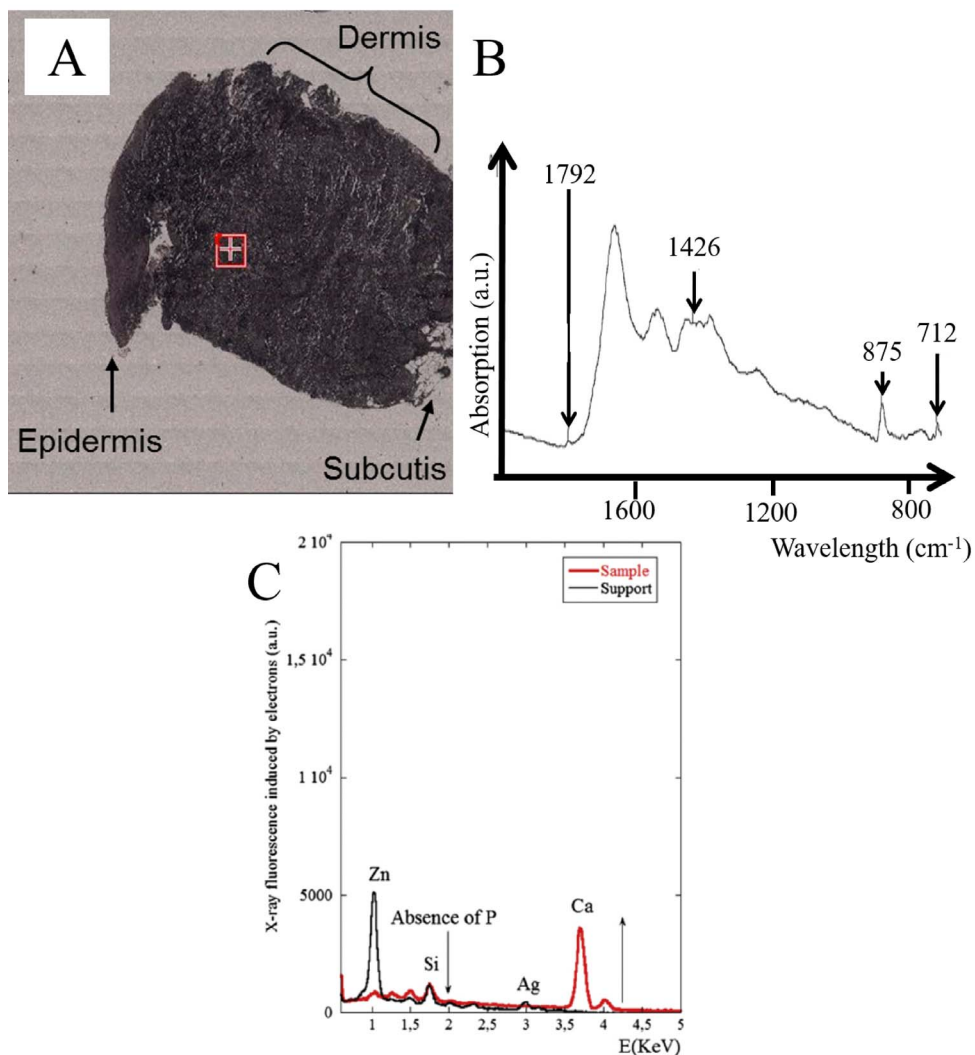
Figure 13. (A) Optical photograph of skin sarcoidosis; (B) Infrared spectrum of the peaks characteristic of calcite (1087 cm^{-1} (weak), 881 cm^{-1}, 1432 cm^{-1}, 712 cm^{-1}) in a protein matrix, from the area corresponding to the red square on the map, located in the dermis. (C) Electron induced X-ray fluorescence of the sample. The contributions of trace elements from the support, namely Zn (1.01 keV), Si (1.74 keV) and Ag (2.98 keV), are clearly visible.

troscopy to identify the organic compounds present in tattoo inks [170–173]. As we can see in Figure 15, the sensitivity of laboratory XRF is sufficient to show the presence of various elements in a skin biopsy. The micrometre resolution of Raman spectroscopy enabled the identification of an organic compound, namely the Pigment Red 170 (PR170) dye, as well as agglomerates of TiO$_2$ nanoparticles (Figure 16). Even though it is usually possible to define the chemical

nature of iron oxide [174,175], this approach was not possible with our sample, probably due to a lack of sensitivity.

Like other researchers working on tattoos [176, 177], we also used synchrotron characterization techniques, specifically XANES spectroscopy where acquisition at the iron K edges (Figure 17) defines the iron environment.

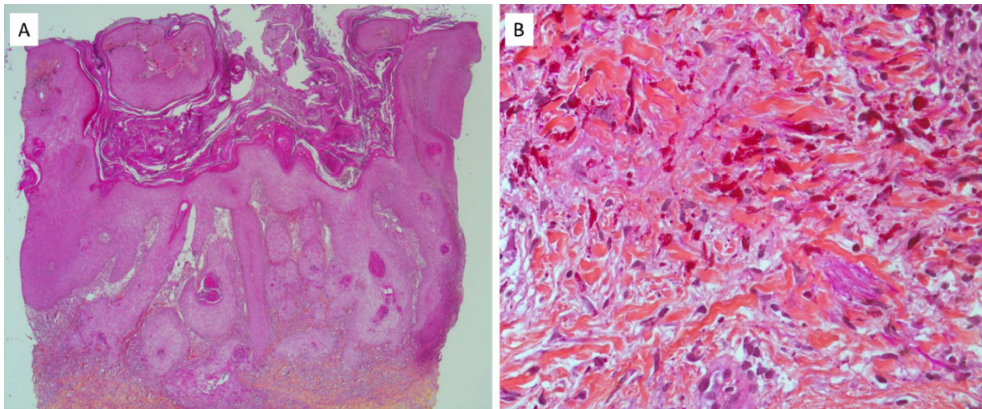While Ti always has an exogenous origin, iron and

Figure 14. Optical microscopy of a KA developed on a tattoo made of red ink, from one of the three patients previsously described. (A) HES ×25. (B) Superficial dermis, HES ×400.
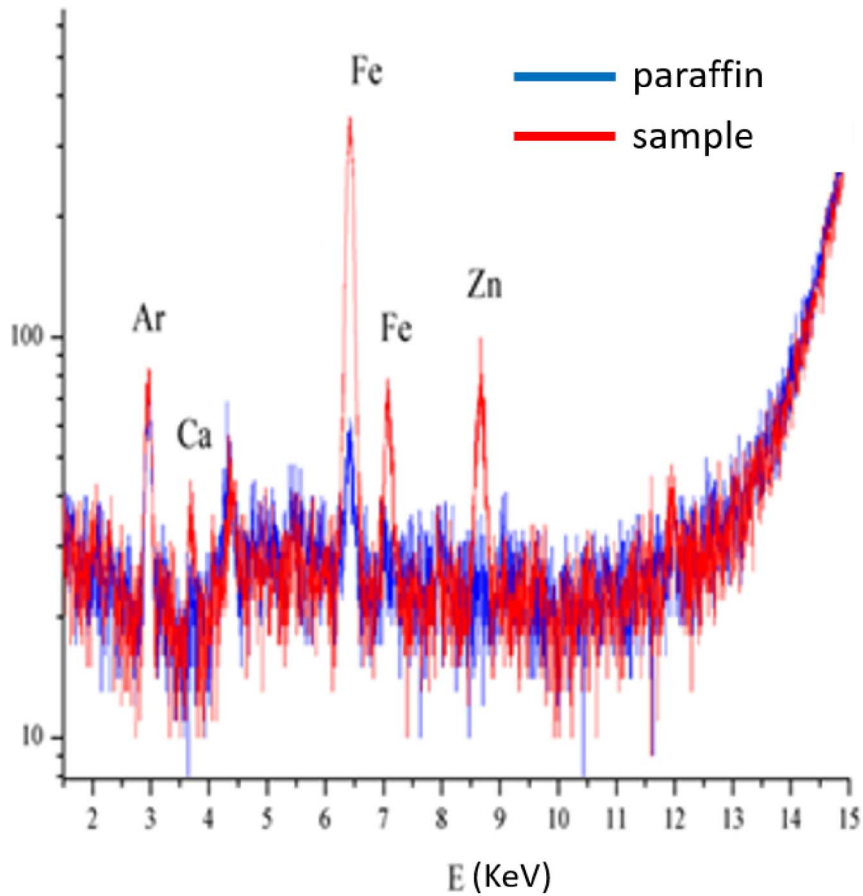

Figure 15. Laboratory XRF spectra of skin reaction to a tattoo. The sample contains high levels of iron and zinc which may be of exogenous or endogenous origin.
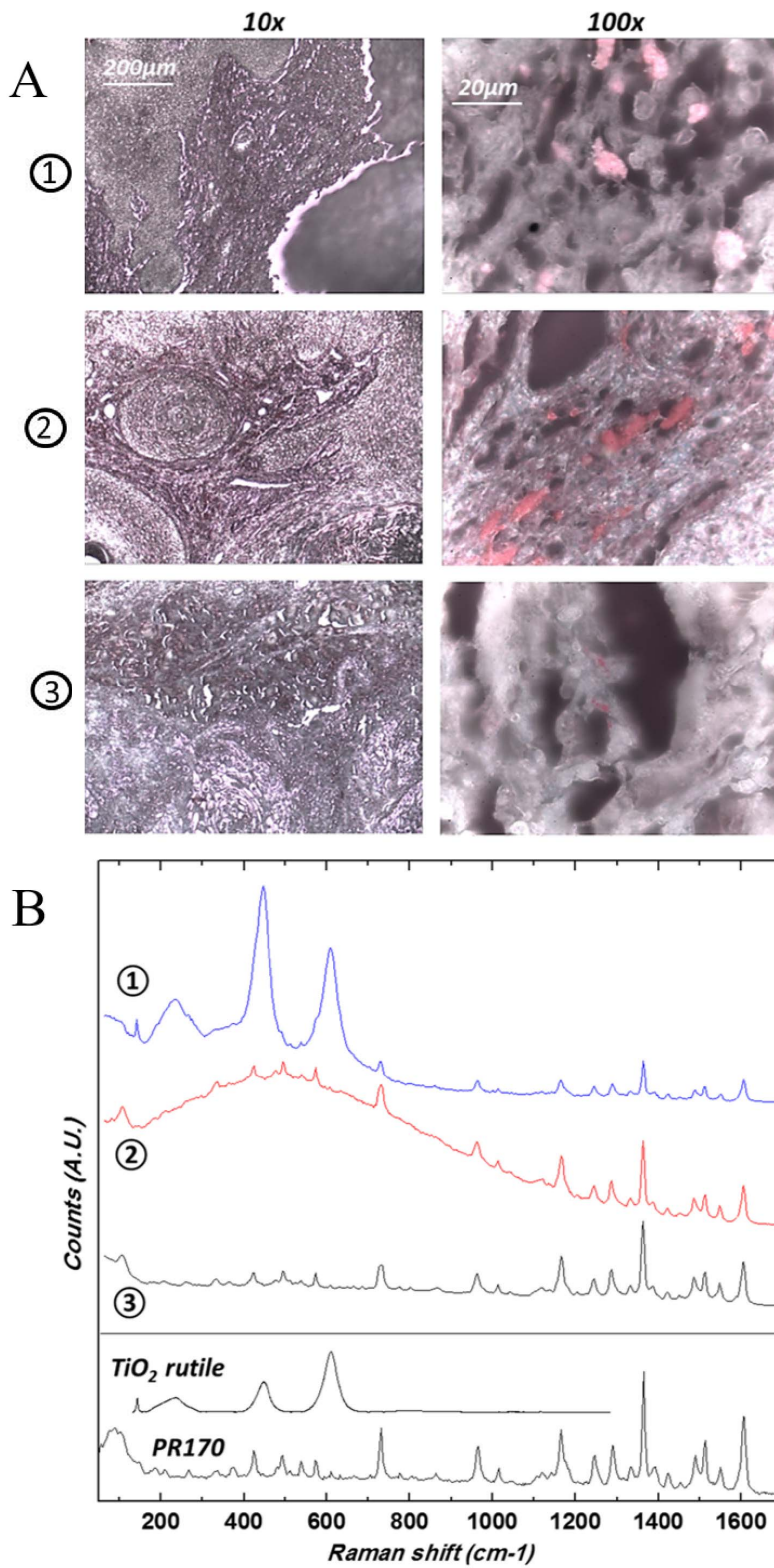
Figure 16. Caption continued on next page.

Figure 16 (cont.). (A) Optical micrographs of the samples of the three patients previously described, at two different magnifications (10× and 100×) revealing micron size red pigment clusters. In patient 1, note the heterogenous and lighter aspect of the red pigment, suggesting the presence of nanoparticles of TiO_2. (B) Corresponding Raman spectra. Reference spectra are also given as a comparison: PR170 dye sample (Kremer) and rutile (TiO_2) downloaded from the RRUFF database.

Table 3. Synthetic iron oxide (found in pigments)

Name	Formula	Colour
Hematite	Fe_2O_3	Red
Magnetite	Fe_3O_4	Black
Goethite	$FeO(OH)$	Yellow
Limonite	$Fe_2O_3\,H_2O$	Brown

Table 4. Synthetic compounds used as pigments

Colour	Ingredients
Black	Magnetite
Red	Iron oxide/common rust, ferric sulfate, hematite,
Green	Ferrocyanide and ferro-ferric cyanide,
Blue	Ferric ferrocyanide

zinc can be either exogenous or endogenous. XANES spectroscopy can be used to chemically characterize these elements; for example, in the case of iron, XANES spectra of human adult deoxyhaemoglobin and myoglobin have been measured [178]. For exogenous iron, among the different compounds which have been identified in pigments, H. Petersen and D. Lewe noticed the presence of the following oxides: Fe_2O_3, $FeO(OH)$ and Fe_3O_4 [176]. Table 3 summarizes synthetic iron oxides used as pigments [179]. Islam *et al.* [180] reported other chemical compounds containing iron (Table 4). As we can see, ferric sulfate, ferric ferrocyanide (the anion $[Fe(CN)_6]^{4-}$) and ferricyanide (the anion $[Fe(CN)_6]^{-3}$) may be also present. Most of the particles used in pigments can be considered to be nanomaterials [181].

Other elements in tattoo ink are associated with the iron or titanium. For example, as underlined by Prior [153,154], all iron oxide pigments contain minor amounts of nickel impurities, even when iron oxide pigments are refined to a high degree of purity. The fact that nickel incorporates into the crystal structure constitutes a health risk of possible allergic reactions [153,154].

Figure 17 shows the spatial repartition of iron in a KA developed on tattoo ink. When we compare the experimental Xanes spectra of the selected POI with that ofv goethite, it is quite clear that this compound has been used.

4.4. *Frontal fibrosing alopecia*

Fibrosing frontal alopecia (FFA) was first described 20 years ago. It is characterized by scarring alopecia on the anterior area of the scalp and mainly affects women after menopause [182]. Its origin is unknown, but as the number of cases continues to increase, it is suspected that extraneous compounds found in leave-on facial skin care products are implicated [183]. TiO_2 is the most widely used white pigment. It is found in a very large number of products: paints, construction materials, food (candies, cookies, etc.), pharmaceuticals (capsule shell, toothpaste, etc.) but also in cosmetics: creams and sunscreens, due to the UV blocking properties of TiO_2. The potential toxicity of TiO_2 is currently a major public health concern—TiO_2 has been classified in group 2B ("possibly carcinogenic to humans") by the International Agency for Research on Cancer; the long-term dermatological impact of these particles is not yet well known in humans. It is still debated whether TiO_2 penetrates the stratum corneum, but it has been clearly demonstrated that it can be deposited in the follicular orifice [184].

In a previous publication, we reported finding titanium dioxide (TiO_2) nanoparticles along the hair follicles of a patient with FFA, who had been using daily sunscreens containing TiO_2 for years [104]. The analyses were carried out by electron microscopy, and by X-ray fluorescence spectroscopy at the Nanoscopium beamline (Figure 18). First, a search for nanoparticles was carried out by scanning electron microscopy coupled with energy dispersive X-ray absorption
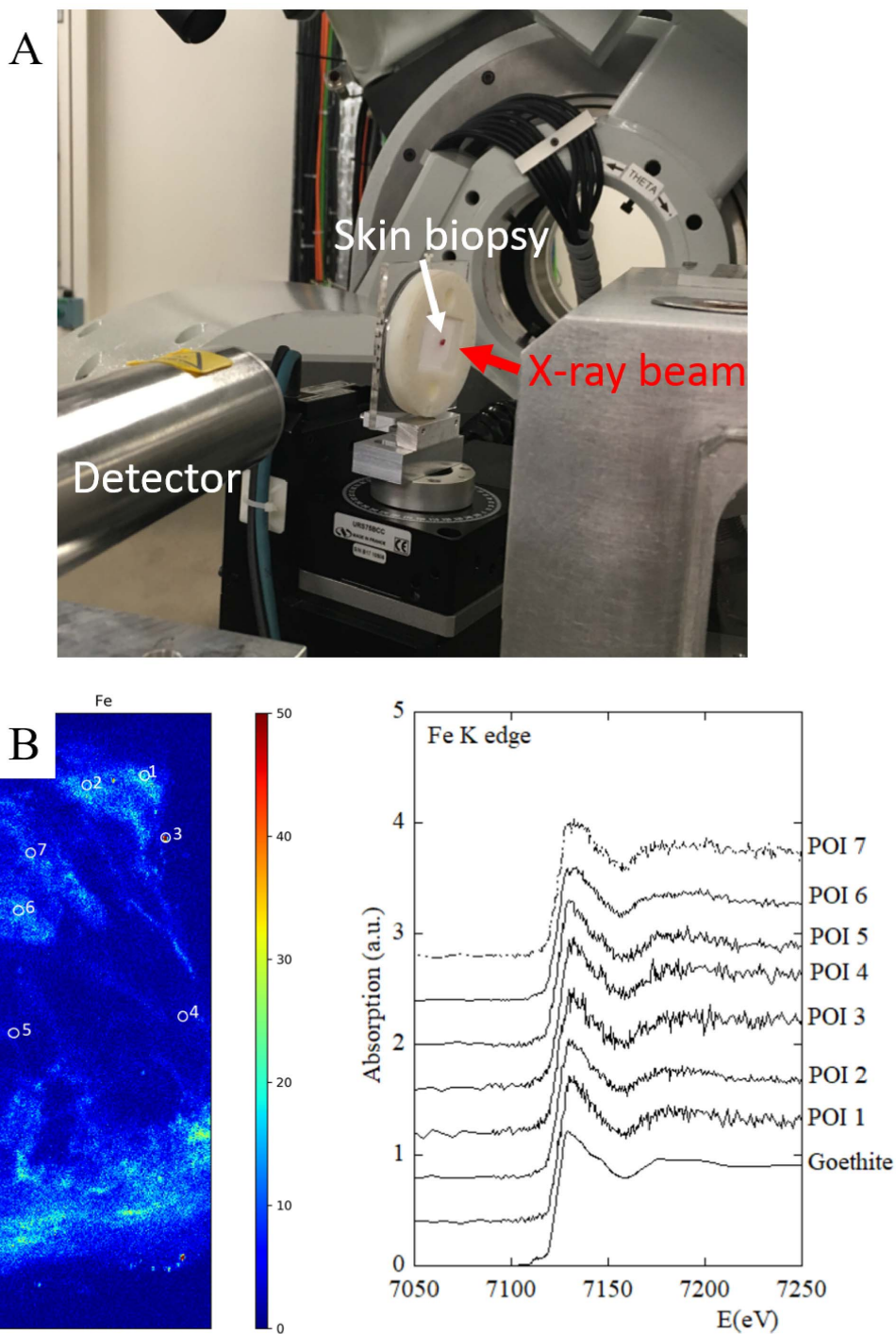
Figure 17. (A) Xanes spectroscopy set-up at Synchrotron Soleil, Diffabs beam line. (B) XANES spectroscopy at the Fe K-edge: XANES spectra at Fe K-edge were acquired at 7 points of interest (POI) in order to characterize the Fe environment.
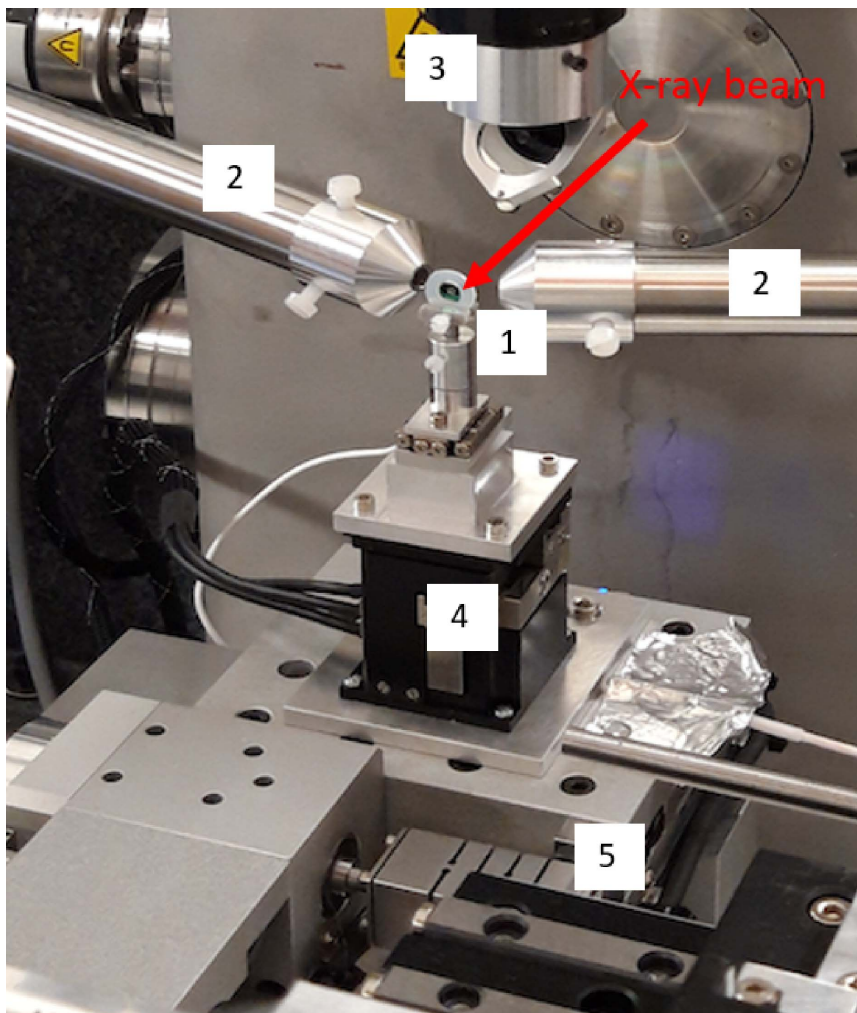
Figure 18. Nanoscopium set up. 1: Sample. 2: X-Ray fluorescence detectors. 3: Visible microscope for sample alignement. 4: Nanopositioning for high spatial resolution. 5: Stepper motors for large field of view.

spectroscopy. Abnormal deposits, micrometric in size, were observed along the hair and their analysis revealed that they contained titanium.

To refine these results, the deposits were studied on the Nanoscopium beamline of the Synchrotron Soleil by fluorescence spectroscopy using an X-ray nanobeam (300×300 nm^2), in order to obtain elemental maps of several areas of these deposits [185]. Figure 19 shows a typical X-ray fluorescence spectrum in which contributions of different elements appear, namely S, Ca, Ti, Fe, Zn and Br.

As we can see on Figure 19, XRF spectroscopy is able to detect different elements in biopsy [186,187]

and thus can play a major role in metal intoxication [188]. Here we would like to consider three of them namely sulfur, zinc and titanium and thus discuss health problems not connected to pathological calcifications. X-ray Sulfur detection in human hair fibers (Figure 19) is due to the fact that hair is primarily composed of keratin proteins with a very high content of cysteine, a sulfur-containing amino acid, which commonly forms cystine via a disulfide bond [189,190]. The detection of sulfur in hair by XRF and XANES in dementia has been discussed, for example by Siritapetawee *et al.* [191] in the context of possible roles of calcium, chlorine, phosphorus and
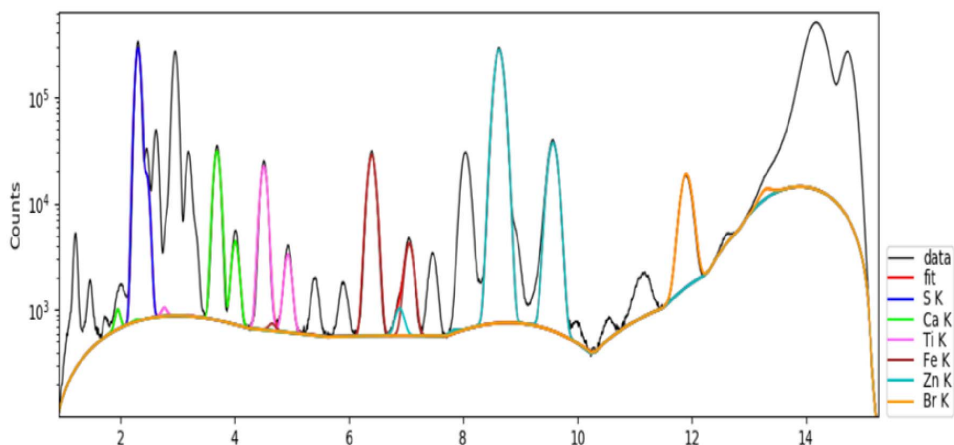
Figure 19. Typical X-ray fluorescence spectrum collected from a hair with the contributions of S (K_α at 2.31 keV, K_β at 2.46 keV), Ca (K_α at 3.69 keV, K_β at 4.01 keV) Ti (K_α at 4.51 keV, K_β at 4.93 keV), Fe (K_α at 6.40 keV, K_β at 7.06 keV), Zn (K_α at 8.638 keV, K_β at 9.572 keV) and Br (K_α at 11.92 keV, K_β at 13.29 keV).
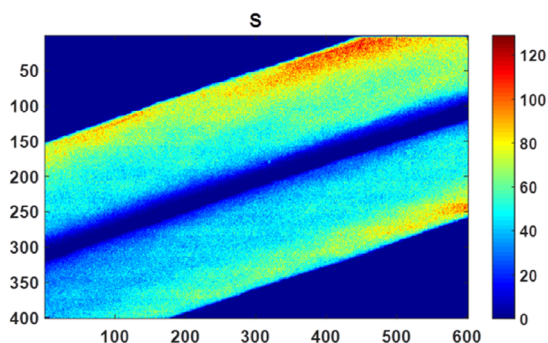

Figure 20. Micro X-ray fluorescence spectroscopy: high 500 nm resolution distribution maps of sulfur (S) within a hair shaft.

sulfur in the etiology of elderly patients' dementia. Also, Inoue *et al.* [189] showed that it is possible to map the oxidation state of cysteine in human hair through Xanes spectroscopy. In our experiment (Figure 20), it is quite clear that the nanometer scale resolution allows us to precisely define the distribution of sulfur in hair.

Numerous publications have discussed the presence of Zn in hairs. A first investigation performed by Bertazzo *et al.* [192] determined the Cu and Zn levels of both 607 men (1–85 y old) and 649 women (1–92 y old) by atomic absorption spectrometry. These authors noticed that sex does not influence Zn content

(200.97 ± 9.68 μg/g for men and 209.81 ± 9.49 μg/g hair for women). Subsequently Dastgheib *et al.* [193] investigated the relationship between alopecia areata (AA) and iron, zinc, and copper levels in serum and hair. According to their data, there was no statistically significant difference between trace elements among AA patients and control patients. Such a conclusion is not in line with Ozaydin-Yavuz *et al.*'s publication [194]. These authors found that low levels of Zn and Mn are associated with AA while other metals were normal: Zn supplementation may therefore have some beneficial effect in AA. In our case, it is quite difficult to extract a conclusion regarding the spatial repartition of Zn in hairs (Figure 21). As underlined by Nicolis *et al.* [195], the usual techniques applied to human hair analysis yield a mean concentration, whilst the analysis of a single hair reveals important fluctuations in three levels: with time (along the hair), between the hairs of the same person, as well as between the hairs of different people.

Finally, it is worth noting that various shampoos contain zinc; clinical studies have established that Zn pyrithione is one of the most effective anti-dandruff ingredients in shampoo formulations [189–191,196].

We paid particular attention to Ti. TiO_2 microparticles (0.5–1 μm) were detected along the surface of follicles thanks to the high sensitivity of the Nanoscopium beamline (Figure 22).

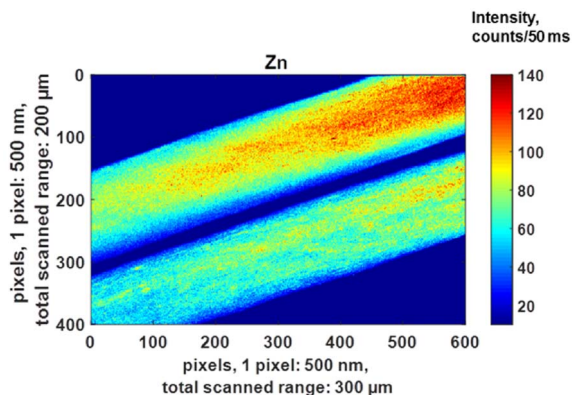As in tattoo associated KA, we have also used Ra-

Figure 21. Micro X-ray fluorescence spectroscopy: high 500 nm resolution distribution maps of Zn within a hair shaft.

man spectroscopy in FFA, allowing us to both localize TiO_2 and identify its crystalline form i.e. whether anatase or rutile (Figure 23).

The hypothesis formulated by the researchers to explain FFA is that TiO_2 provokes an inflammatory reaction [192–194,197–199]. Up to now, there is no data available concerning the impact of TiO_2 exposure on hair. However, the detection of TiO_2 along the hair shafts of our patient raises the question of possible implication of TiO_2 in FFA pathogenesis: these inflammatory reactions, when occurring in the bulge of the hair follicle, could lead to the destruction of the stem cells located within the bulge. Dynamic studies on hair follicles extracted after application of cream containing TiO_2, with measurements of nanoparticles on different parts of the hair follicle, as well as more detailed analyses to characterize the exact location of the nanoparticles, are necessary to confirm the potential link between FFA and TiO_2 nanoparticles.

5. *In vivo* characterization

In vivo characterization is a promising approach for the clinican. Among those physiocochemical characterization techniques able to collect data on skin *in vivo* are Raman spectroscopy [195,200–203], FTIR spectroscopy [204,205], X-ray fluorescence [206,207] and Optical Coherence Tomography (OCT). We have used two of these: OCT in sarcoidosis and FTIR spectroscopy on tattoos.

OCT is a technology based on low-coherence optical interferometry to image biological tissues with a micrometer-scale spatial resolution [208,209]. It is commonly used in several medical fields [210], especially in ophthalmology to obtain images of the retina and the anterior segment of the eye [211]. Moreover, OCT has begun to be used in interventional cardiology [212], and in gastro-enterology for the detection and diagnosis of tumors [213,214]. OCT can be a useful tool for non-invasive imaging of brain tissues [215,216], and shows promise in dermatology to improve the diagnosis of skin lesions [217,218].

In this study, we used a commercially available swept-source OCT device (Thorlabs, OCS1300SS) operating in the near-infrared at a center wavelength of 1300 nm, producing images with a spatial resolution of 12 μm × 25 μm (axial × transverse). Figure 24 shows an example of an OCT image obtained from a biopsy of skin sarcoidosis embedded in paraffin. OCT is effective in identifying granulomas in the dermis, suggesting that this technique could also be used to diagnose cutaneous sarcoidosis *in vivo*, which would prevent the patient from having to undergo a biopsy.

Finally, we have recently tested the acquisition of *in vivo* FTIR spectra using an Agilent 4300 Handheld FTIR spectrometer. The experimental setup, routinely used for archeomaterials [219], allows the acquisition of infrared spectra in the range 5000–650 cm^{-1} with a spectral resolution of 4 cm^{-1}. The detector is thermal and the signal is related to a change in temperature caused by the absorption of the infrared radiation. Experiments were performed in attenuated total reflection mode (with a 2 μm typical penetration depth) using a diamond interface window on a patient with a tattoo. A set of infrared spectra were collected (Figure 25): it is clear that the signal to noise is excellent and thus it seems possible to extract spectral information regarding the chemical composition of the tattoos. Following these preliminary experiments, we have started an investigation in order to analyse quantitatively these IR spectra.

6. Conclusion and perspectives

This contribution exemplifies different physicochemical techniques, encompassing imaging at the submicrometer scale by FE-SEM, chemical identification by two vibrational spectroscopies namely
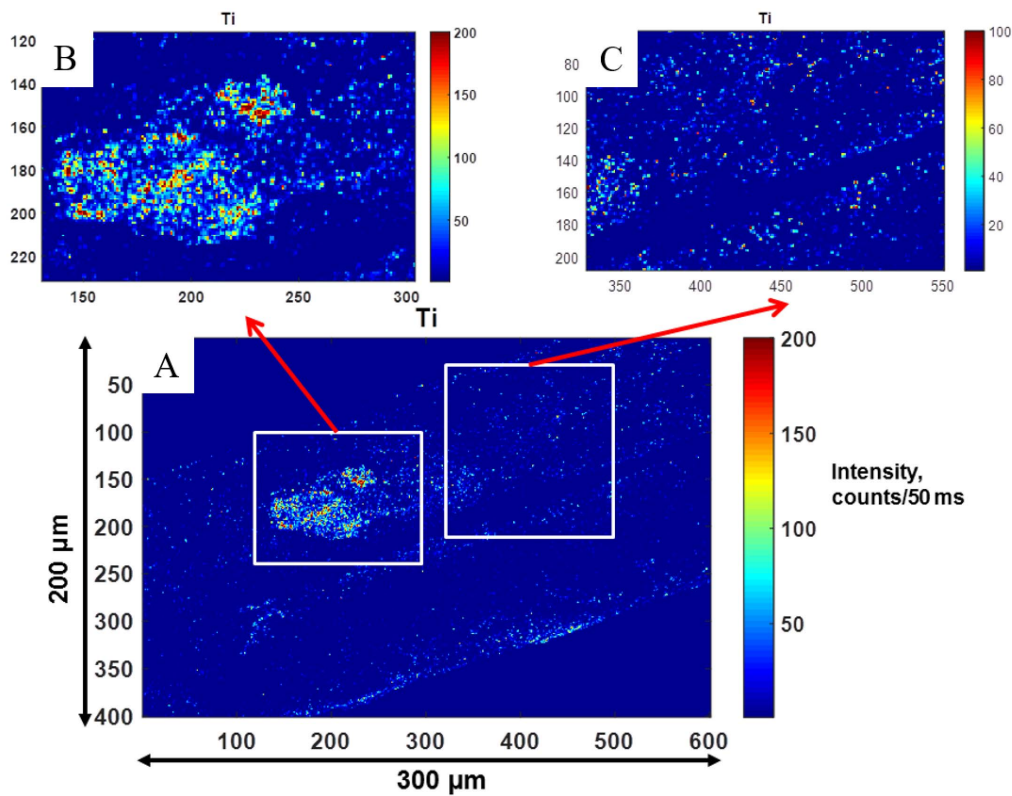
Figure 22. Nano X-ray fluorescence spectroscopy: high 500 nm resolution distribution maps of Ti within a hair sample. Red color areas correspond to a high concentration of Ti.

FTIR and Raman, as well as techniques specific to synchrotron radiation such as XRF and XANES, have been used to describe both endogenous and exogenous skin deposits.

The complete set of results demonstrates clearly that, although carbapatite is usually identified in endogenous deposits, various other chemical compounds can be identified. Such chemical diversity in skin calcifications suggests different biochemical mechanisms. We have also demonstrated the variety of structures and locations adopted by such skin deposits.

Regarding exogenous skin deposits, we identified PAA and metal oxides in KA, which were strongly correlated with the position of the tumour, and identified TiO_2 in FFA, which was closely located next to the area rich in stem cells of the hair follicle. This co-localization suggests a direct involvement of these compounds in these diseases.

In the near future, we would like to apply other tools in various skin diseases. Nowadays, it is possible to perform a description of the pathological calcifications at the nanometer scale. Transmission electron microscopy (TEM) has already been used and such description has led to different scientific breakthroughs [220–222]. Combining TEM and electron energy loss experiments tells the clinician the morphology and the elemental composition of abnormal tissue deposits at the nanometre scale [223,224]. There is also now the possibility of identifying chemical composition by the acquisition of NanoInfrared spectra [225–228].

Other tools, such as UV spectroscopy [229–231] or Second Harmonic Generation (SHG) [232–234] are also very interesting for the exploration of skin diseases. We have obtained promising preliminary results at the Disco beamline, Synchrotron Soleil, and we will proceed with more analyses in the future. Figure 26 shows as an example of spontaneous fluorescence within sweat glands (red arrow).
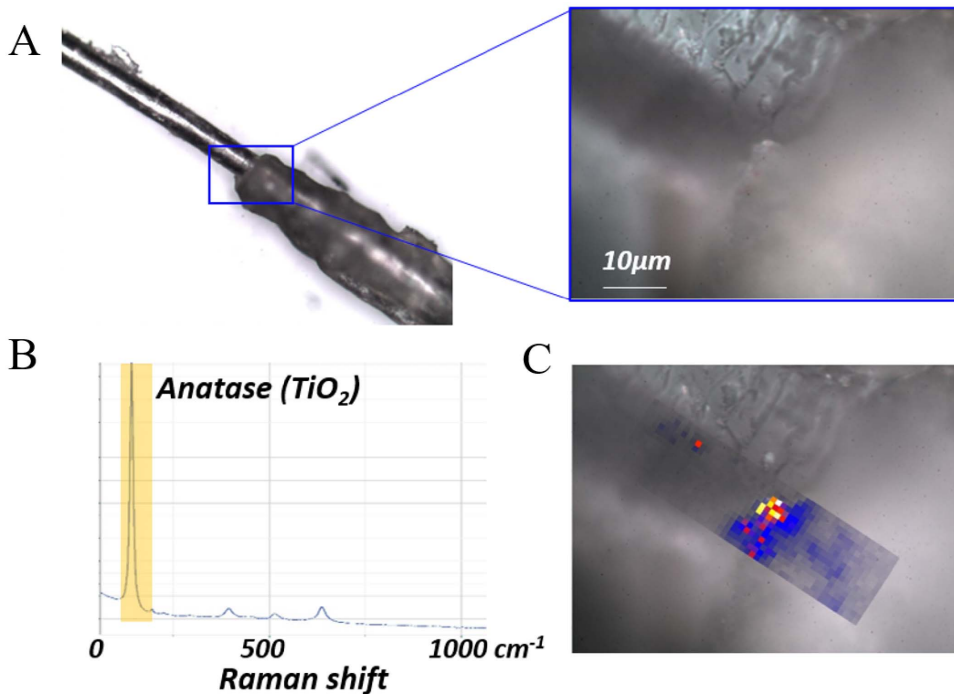
Figure 23. Raman characterization of a hair follicle from a patient with frontal fibrosing alopecia: (a) Optical micrograph at 10× and 100× magnification, (b) Raman spectrum (785 nm, laser power: 22.5 mW Acq. time = 0.5 s) revealing the presence of anatase and (c) Raman mapping by integration of the intensity of the 142 cm^{-1} band of anatase over the energy range 120–160 cm^{-1}, showing a high concentration of anatase at the hair/follicle junction.
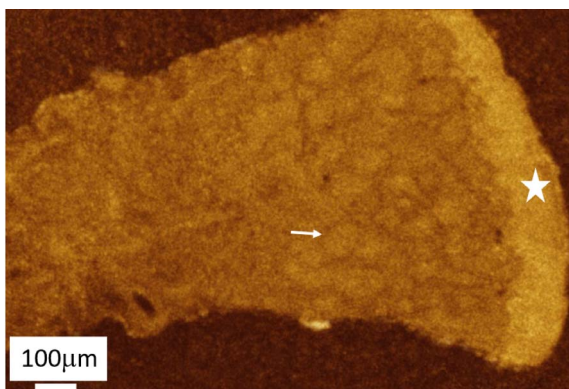

Figure 24. OCT analysis in skin sarcoidosis: epidermis (dot), dermis and clear visualisation of many granulomas (arrow).

Synchrotron radiation provides other opportunities for nanometer scale definition. For example, scanning transmission X-ray microscopy performed at the carbon K-edge and at the Ca L$_{2,3}$-edges can accurately assess the pathogenesis of calcifications inside bacteria [235].

Finally, all these nanometer scale experimental data have to be considered via a "bottom-up" approach based on DFT model chemistry [236–238]. Such a theoretical approach can model different kinds of apatite/biomolecule [239–241] and metal or metal oxide/small molecule interactions [242–244] which can have a major influence in the case of tattoos.

Further collaborations and studies are therefore projected, including multiphoton microscopy analyses, in order to provide a better understanding of skin diseases associated with endogenous and exogenous deposits, and hopefully improve their treatment.
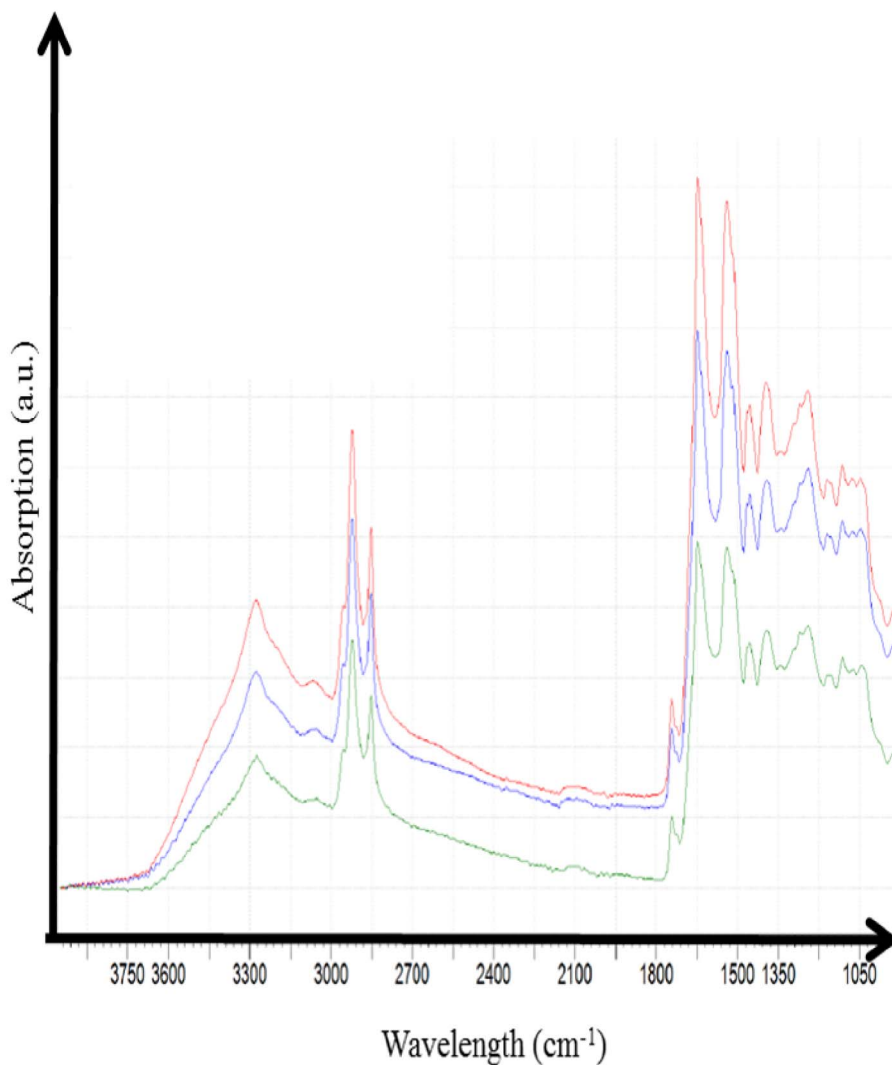
Figure 25. *In vivo* infrared spectra of a skin tattoo acquired with a portable infrared experimental setup.

Conflicts of interest

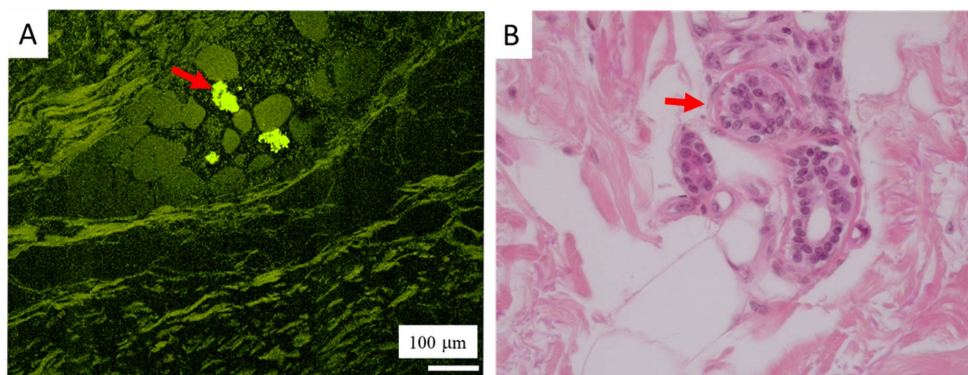Authors have no conflict of interest to declare.

Figure 26. Comparison of SHG and optical microscopy. (A) Spontaneous fluorescence is observed within sweat glands (red arrow), here surrounded by adipocytes. (B) HES ×400, sweat glands (red arrow), also surrounded by adipocytes.

References

[1] D. Bazin, M. Daudon, C. Combes, C. Rey, *Chem. Rev.*, 2012, **112**, 5092-5120.

[2] D. Bazin, M. Daudon, *J. Phys. D: Appl. Phys.*, 2012, **45**, article no. 383001.

[3] L. N. Poloni, M. D. Ward, *Chem. Mater.*, 2014, **26**, 477-495.

[4] E. Tsolaki, S. Bertazzo, *Materials*, 2019, **12**, article no. 3126.

[5] D. Bazin, M. Daudon, *J. Spectral Imaging*, 2019, **8**, article no. a16.

[6] N. Vidavsky, J. A. M. R. Kunitake, L. A. Estroff, *Adv. Healthc. Mater.*, 2020, article no. e2001271.

[7] A. M. Molina-Ruiz, L. Cerroni, H. Kutzner, L. Requena, *Am. J. Dermatopathol.*, 2014, **36**, 1-48.

[8] F. Rongioletti, "Exogenous cutaneous deposits with special consideration to skin reactions to soft-tissue fillers", in *Clinical and Pathological Aspects of Skin Diseases in Endocrine, Metabolic, Nutritional and Deposition Disease* (B. Smoller, F. Rongioletti, eds.), Springer, New York, NY, 2010.

[9] M.-T. Liu, W.-T. Cheng, M.-J. Li, H.-N. Liu, D.-M. Yang, S.-Y. Lin, *Arch. Dermatol. Res.*, 2005, **297**, 231-234.

[10] V. Rafnsson, O. Ingimarsson, I. Hjalmarsson, H. Gunnarsdottir, *Occup. Environ. Med.*, 1998, **55**, 657-660.

[11] L. F. Bonewald, S. E. Harris, J. Rosser, M. R. Dallas, S. Dallas, N. P. Camacho, B. Boyan, A. Boskey, *Calcif. Tissue Int.*, 2003, **72**, 537-547.

[12] M. Daudon, D. Bazin, "New techniques to characterize kidney stones and Randall's plaque", in *Urolithiasis: Basic Science and Clinical Practice* (J. J. Talati, H. G. Tiselius, D. M. Albala, Z. Ye, eds.), Springer, London, 2012, 683-707.

[13] D. Bazin, Ch. Jouanneau, S. Bertazzo, Ch. Sandt, A. Dessombz, M. Réfrégiers, P. Dumas, J. Frederick, J.-Ph. Haymann, E. Letavernier, P. Ronco, M. Daudon, *C. R. Chim.*, 2016, **19**, 1439-1454.

[14] V. Frochot, D. Bazin, E. Letavernier, Ch. Jouanneau, J.-Ph. Haymann, M. Daudon, *C. R. Chim.*, 2016, **19**, 1565-1572.

[15] H. Bilbault, J. Perez, L. Huguet, S. Vandermeersch, S. Placier, N. Tabibzadeh, V. Frochot, E. Letavernier, D. Bazin, M. Daudon, J.-P. Haymann, *Sci. Rep.*, 2018, **8**, article no. 16319.

[16] A. Dessombz, P. Méria, D. Bazin, M. Daudon, *PLoS One*, 2012, **7**, article no. e51691.

[17] A. Dessombz, P. Méria, D. Bazin, E. Foy, S. Rouzière, R. Weil, M. Daudon, *Prog. Urol.*, 2011, **21**, 940-945.

[18] M. Mathonnet, A. Dessombz, D. Bazin, R. Weil, F. Triponez, M. Pusztaszeri, M. Daudon, *C. R. Chim.*, 2016, **19**, 1672-1678.

[19] J. Guerlain, S. Perie, M. Lefevre, J. Perez, S. Vandermeersch, Ch. Jouanneau, L. Huguet, V. Frochot, E. Letavernier, R. Weil, S. Rouziere, D. Bazin, M. Daudon, J. P. Haymann, *PLoS One*, 2019, **14**, article no. e0224138.

[20] F. Brisset, M. Repoux, J. Ruste, F. Grillon, F. Robaut, *Microscopie Electronique à Balayage et Microanalyses*, EDP Sciences, Les Ulis, 2009.

[21] D. Bazin, M. Daudon, *Ann. Biol. Clin.*, 2015, **73**, 517-534.

[22] D. Bazin, E. Bouderlique, M. Daudon, V. Frochot, J.-Ph. Haymann, E. Letavernier, F. Tielens, R. Weil, *C. R. Chim.*, 2022, **25**, no. S1, 37-60.

[23] A. Dessombz, C. Nguyen, H.-K. Ea, S. Rouzière, E. Foy, D. Hannouche, S. Réguer, F.-E. Picca, D. Thiaudière, F. Lioté, M. Daudon, D. Bazin, *J. Trace Elem. Med. Biol.*, 2013, **27**, 326-333.

[24] S. Rouzière, D. Bazin, M. Daudon, *C. R. Chim.*, 2016, **19**, 1404-1415.

[25] D. Bazin, E. Foy, S. Reguer, S. Rouzière, B. Fayard, H. Colboc, J.-Ph. Haymann, M. Daudon, C. Mocuta, *C. R. Chim.*, 2022, **25**, no. S1, 165-188.

[26] A. Guinier, *Théorie et technique de la radiocristallographie*, Dunod, Paris, 1964.

[27] D. Bazin, C. Chappard, C. Combes, X. Carpentier, S. Rouzière, G. André, G. Matzen, M. Allix, D. Thiaudière, S. Reguer, P. Jungers, M. Daudon, *Osteoporos. Int.*, 2009, **20**, 1065-1075.

[28] S. Reguer, C. Mocuta, D. Thiaudière, M. Daudon, D. Bazin, *C. R. Chim.*, 2016, **19**, 1424-1431.

[29] D. Bazin, V. Frochot, J.-Ph. Haymann, E. Letavernier, M. Daudon, *C. R. Chim.*, 2022, **25**, no. S1, 133-147.

[30] N. Quy Dao, M. Daudon, *Infrared and Raman Spectra of Calculi*, Elsevier, Paris, 1997.

[31] L. Estepa, M. Daudon, *Biospectroscopy*, 1997, **3**, 347-369.

[32] S. Y. Lin, *Expert Rev. Mol. Med.*, 2014, **16**, article no. e6.

[33] M. Daudon, D. Bazin, *C. R. Chim.*, 2016, **19**, 1416-1423.

[34] I. T. Lucas, D. Bazin, M. Daudon, *C. R. Chim.*, 2022, **25**, no. S1, 83-103.

[35] S. Tamosaityte, M. Pucetaite, A. Zelvys, S. Varvuolyte, V. Hendrixson, V. Sablinskas, *C. R. Chim.*, 2022, **25**, no. S1, 73-82.

[36] D. Bazin, M. Daudon, P. Chevallier, S. Rouzière, E. Elkaim, D. Thiaudière, B. Fayard, E. Foy, P. A. Albouy, G. André, G. Matzen, E. Véron, *Ann. Biol. Clin. (Paris)*, 2006, **64**, 125-139.

[37] D. Bazin, J.-Ph. Haymann, E. Letavernier, J. Rode, M. Daudon, *Presse Med.*, 2014, **43**, 135-148.

[38] M. Daudon, D. Bazin, *J. Phys.: Conf. Ser.*, 2013, **425**, article no. 022006.

[39] D. Bazin, E. Letavernier, J.-P. Haymann, P. Méria, M. Daudon, *Prog. Urol.*, 2016, **26**, 608-618.

[40] D. E. Sayers, F. W. Lytle, E. A. Stern, *Adv. X-ray Anal.*, 1970, **13**, 248-271.

[41] J. J. Rehr, A. L. Ankudinov, *Coord. Chem. Rev.*, 2005, **249**, 131-140.

[42] D. Bazin, D. Sayers, J. Rehr, *J. Phys. Chem. B*, 1997, **101**, 11040-11050.

[43] D. Bazin, D. Sayers, J. J. Rehr, C. Mottet, *J. Phys. Chem. B*, 1997, **101**, 5332-5336.

[44] D. Bazin, J. J. Rehr, *J. Phys. Chem. B*, 2003, **107**, 12398-12402.

[45] D. Bazin, S. Reguer, D. Vantelon, J.-Ph. Haymann, E. Letavernier, V. Frochot, M. Daudon, E. Esteve, H. Colboc, *C. R. Chim.*, 2022, **25**, no. S1, 189-208.

[46] D. Bazin, E. Letavernier, J. P. Haymann, V. Frochot, M. Daudon, *Ann. Biol. Clin.*, 2020, **78**, 349-362.

[47] M. Daudon, P. Jungers, D. Bazin, *New England J. Med.*, 2008, **359**, 100-102.

[48] D. Bazin, G. André, R. Weil, G. Matzen, E. Véron, X. Carpentier, M. Daudon, *Urology*, 2012, **79**, 786-790.

[49] A. Dessombz, E. Letavernier, J.-Ph. Haymann, D. Bazin, M. Daudon, *J. Urol.*, 2015, **193**, 1564-1569.

[50] S. Kaščáková, C. M. Kewish, S. Rouzière, F. Schmitt, R. Sobesky, J. Poupon, C. Sandt, B. Francou, A. Somogyi, D. Samuel, E. Jacquemin, A. Dubart-Kupperschmitt, T. H. Nguyen, D. Bazin, J.-C. DuclosVallée, C. Guettier, F. Le Naour, *J. Pathol. Clin. Res.*, 2016, **2**, 175-186.

[51] D. Bazin, M. Daudon, G. André, R. Weil, E. Véron, G. Matzen, *J. Appl. Crystallogr.*, 2014, **47**, 719-725.

[52] N. Reiter, L. El-Shabrawi, B. Leinweber, A. Berghold, E. Aberer, *J. Am. Acad. Dermatol.*, 2011, **65**, 14-15.

[53] J. S. Walsh, J. A. Fairley, *J. Am. Acad. Dermatol.*, 1995, **33**, 693-706.

[54] A. Valenzuela, L. Chung, *Curr. Treat Options Rheumatol.*, 2016, **2**, 85-96.

[55] A. G. Tristano, J. L. Villarroel, M. A. Rodríguez, A. Millan, *Clin. Rheumatol.*, 2006, **25**, 70-74.

[56] B. C. Presley, J. S. Bush, S. C. Watson, *West J. Emerg. Med.*, 2012, **13**, 136-138.

[57] O. Le Saux, Z. Urban, C. Tschuch, K. Csiszar, B. Bacchelli, D. Quaglino, I. Pasquali-Ronchetti, F. Michael Pope, A. Richards, S. Terry, L. Bercovitch, A. de Paepe, C. D. Boyd, *Nat. Genet.*, 2000, **25**, article no. 223.

[58] S. E. Lee, S. Hun, *Ann. Dermatol.*, 2018, **30**, 265-275.

[59] A. B. G. Lansdown, *Wound Rep. Reg.*, 2002, **10**, 271-285.

[60] M. P. Adams, D. G. Mallet, G. J. Pettet, *PLoS One*, 2015, **10**, article no. e0116751.

[61] P. Henrot, A. Leroux, C. Barlier, P. Génin, *Diagn. Interv. Imaging*, 2014, **95**, 141-152.

[62] A. B. Lakhdar, M. Daudon, M. C. Mathieu, A. Kellum, C. Balleyguier, D. Bazin, *C. R. Chim.*, 2016, **19**, 1610-1624.

[63] H. Colboc, Ph. Moguelet, D. Bazin, P. Carvalho, A.-S. Dillies, G. Chaby, H. Maillard, D. Kottler, E. Goujon, Ch. Jurus, M. Panaye, V. Frochot, E. Letavernier, M. Daudon, I. Lucas, R. Weil, Ph. Courville, J.-B. Monfort, F. Chasset, P. Senet, *JAMA Dermatol.*, 2019, **155**, 789-796.

[64] L. M. Pachman, A. Veis, S. Stock, K. Abbott, F. Vicari, P. Patel, D. Giczewski, C. Webb, L. Spevak, A. L. Boskey, *Arthritis Rheumatol.*, 2006, **54**, 3345-3350.

[65] R. Kramann, V. M. Brandenburg, L. J. Schurgers, M. Ketteler, S. Westphal, I. Leisten, M. Bovi, W. Jahnen-Dechent, R. Knüchel, J. Floege, R. K. Schneider, *Nephrol. Dial. Transplant.*, 2013, **28**, 856-868.

[66] T. Ogino, T. Suzuki, K. Sawada, *Geochim. Cosmochim. Acta*, 1987, **51**, 2757-2767.

[67] J. D. Reid, M. E. Andersen, *Am. J. Clin. Pathol.*, 1988, **90**, 545-585.

[68] C. J. Cros, D. Bazin, A. Kellum, V. Rebours, M. Daudon, *C. R. Chim.*, 2016, **19**, 1642-1664.

[69] J.-K. Yua, H. Pan, Sh.-M. Huang, N.-L. Huang, Ch.-Ch. Yao, K.-M. Hsiao, Ch.-W. Wu, *Asian J. Surg.*, 2013, **36**, 26-35.

[70] S. Kraaij, H. S. Brand, E. H. van der Meij, J.-G. de Visscher, *Med. Oral. Patol. Oral. Cir. Bucal*, 2018, **23**, article no. e540.

[71] J. A. Terzakis, W. J. Eisenmenger, J. J. Reidy, *Am. J. Clin. Pathol.*, 1984, **82**, 236-239.

[72] M. Daudon, H. Bouzidi, D. Bazin, *Urol. Res.*, 2010, **38**, 459-467.

[73] H.-K. Ea, Ch. Nguyen, D. Bazin, A. Bianchi, J. Guicheux, P. Reboul, M. Daudon, F. Lioté, *Arthritis Rheum.*, 2010, **63**, 10-18.

[74] S. De Santis, G. Sotgiu, A. Crescenzi, C. Taffon, A. C. Felici, M. Orsini, *J. Pharm. Biomed. Anal.*, 2020, **190**, article no. 113534.

[75] J. M. Richards, J. A. M. R. Kunitake, H. B. Hunt, A. N. Wnorowski, D. W. Lin, A. L. Boskey, E. Donnelly, L. A. Estroff, J. T. Butcher, *Acta Biomateri.*, 2018, **71**, 24-36.

[76] J. A. M. R. Kunitake, S. Choi, K. X. Nguyen, M. M. Lee, F. He, D. Sudilovsky, P. G. Morris, M. S. Jochelson, C. A. Hudis, D. A. Muller, P. Fratzl, C. Fischbach, A. Masic, L. A. Estroff, *J. Struct. Biol.*, 202, **2018**, 25-34.

[77] Ch. Rey, Ch. Combes, Ch. Drouet, H. Sfihi, A. Barroug, *Mater. Sci. Eng.*, 2007, **C27**, 198-205.

[78] S. Cazalbou, D. Eichert, Ch. Drouet, Ch. Combes, Ch. Rey, *C. R. Paleontol.*, 2004, **3**, 563-572.

[79] M. Iafisco, J. M. Delgado-Lopez, C. Drouet, in *Apatites: Synthesis, Structural Characterization and Biomedical Applications* (M. Iafisco, J. M. Delgado-Lopez, eds.), Nova Science Publishers, New York, 2014, Chapter 2, eBook.

[80] Ch. Combes, S. Cazalbou, Ch. Rey, *Minerals*, 2016, **6**, article no. 34.

[81] I. Russoni de Lima, G. Gomes Alves, C. A. Soriano, A. P. Campaneli, Th. H. Gasparoto, E. S. Ramos Jr., L. Á. de Sena, A. M. Rossi, J. M. Granjeiro, *J. Biomed. Mater. Res. A*, 2011, **98**, 351-358.

[82] D. Bazin, M. Daudon, Ch. Chappard, J. J. Rehr, D. Thiaudière, S. Reguer, *J. Synchrotron Radiat.*, 2011, **18**, 912-918.

[83] D. Bazin, A. Dessombz, Ch. Nguyen, H. K. Ea, F. Lioté, J. Rehr, Ch. Chappard, S. Rouzière, D. Thiaudière, S. Reguer, M. Daudon, *J. Synchrotron Radiat.*, 2014, **21**, 136-142.

[84] X. Carpentier, D. Bazin, Ch. Combes, A. Mazouyes, S. Rouzière, P. A. Albouy, E. Foy, M. Daudon, *J. Trace Elem. Med. Biol.*, 2011, **25**, 160-165.

[85] S. Naray-Szabo, *Z. Kristallogr Kristallgeom Kristallphys Kristallchem*, 1930, **75**, 387-398.

[86] T. J. White, D. Zhi Li, *Acta Crystallogr.*, 2003, **B 59**, 1-16.

[87] J. C. Elliott, *Structure and Chemistry of the Apatites and Other Calcium Orthophosphates*, Elsevier, Amsterdam, 1994.

[88] M. Vallet-Regi, M. J. Gonzalez-Calbet, *Prog. Solid State Chem.*, 2004, **32**, 1-31.

[89] S. Ouizat, A. Barroug, A. Legrouri, C. Rey, *Mater. Res. Bull.*, 2000, **34**, 2279-2289.

[90] Ch. Drouet, Ch. Rey, *Nanostructured Biomaterials for Regenerative Medicine*, Woodhead Publishing Series in Biomaterials, Woodhead Publishing, Cambridge, 2020, 223-254 pages.

[91] C. Rey, J. L. Miquel, L. Facchini, A. P. Legrand, M. J. Glimcher, *Bone*, 1995, **16**, 583-586.

[92] C. K. Loong, Ch. Rey, L. T. Kuhn, Ch. Combes, Y. Wu, S. H. Chen, M. J. Glimcher, *Bone*, 2000, **26**, 599-602.

[93] G. Cho, Y. Wu, J. L. Ackerman, *Science*, 2003, **300**, 1123-1127.

[94] R. Legros, N. Balmain, G. Bonel, *Calcif. Tissue Int.*, 1987, **41**, 137-144.

[95] X. Carpentier, M. Daudon, O. Traxer, P. Jungers, A. Mazouyes, G. Matzen, E. Véron, D. Bazin, *Urology*, 2009, **73**, 968-975.

[96] M. Daudon, D. Bazin, G. André, P. Jungers, A. Cousson, P. Chevallier, E. Véron, G. Matzen, *J. Appl. Crystallogr.*, 2009, **42**, 109-115.

[97] A. S. Prasad, *J. Trace Elem. Med. Biol.*, 2014, **28**, 364-371.

[98] N. Z. Gammoh, L. Rink, *Nutrients*, 2017, **9**, article no. 624.

[99] C. P. Wild, *Cancer Epidemiol. Biomarkers Prev.*, 2005, **14**, 1847-1850.

[100] J. Lademann, H. Weigmann, C. Rickmeyer, H. Barthelmes, H. Schaefer, G. Mueller, W. Sterry, *Skin Pharmacol. Appl. Skin Physiol.*, 1999, **12**, 247-256.

[101] R. G. M. Keijsers, D. A. F. van den Heuvel, J. C. Grutters, *Eur. Respir. J.*, 2013, **41**, 743-751.

[102] B. P. Barna, M. A. Judson, M. J. Thomassen, *Adv. Exp. Med. Biol.*, 2021, **1304**, 39-52.

[103] S. A. Ma, S. Imadojemu, K. Beer, J. T. Seykora, *J. Cutan. Pathol.*, 2017, **44**, 672-676.

[104] F. Brunet-Possenti, L. Deschamps, H. Colboc, A. Somogyi, K. Medjoubi, D. Bazin, V. Descamps, *J. Eur. Acad. Dermatol. Venereol.*, 2018, **32**, e442-e443.

[105] R. Ruiz-Villaverde, P. Fernandez-Crehuet, P. Aguayo-Carreras, J. L. Hernandez-Centeno, C. Cuenca-Barrales, *Sultan Qaboos Univ. Med. J.*, 2018, **18**, e215-e218.

[106] R. Bose, Ch. Sibley, S. Fahim, *SAGE Open Med. Case Rep.*, 2020, **8**, article no. 2050313X20936036.

[107] R. H. Weenig, L. D. Sewell, M. D. Davis, J. T. McCarthy, M. R. Pittelkow, *J. Am. Acad. Dermatol.*, 2007, **56**, 569-579.

[108] S. U. Nigwekar, S. Zhao, J. Wenger, J. L. Hymes, F. Maddux, R. I. Thadhani, K. E. Chan, *J. Am. Soc. Nephrol.*, 2016, **27**, 3421-3429.

[109] S. U. Nigwekar, R. Thadhani, V. M. Brandenburg, *N. Engl. J. Med.*, 2018, **378**, 1704-1714.

[110] Z. Yu, L. Gu, H. Pang, Y. Fang, H. Yan, W. Fang, *Case Rep. Nephrol. Dial.*, 2015, **5**, 77-82.

[111] H.-K. Sin, P.-N. Wong, K.-Y. Lo, M.-W. Lo, S.-F. Chan, K.-C. Lo, Y.-Y. Wong, L.-Y. Ho, W.-T. Kwok, K.-C. Chan, A. K.-M. Wong, S.-K. Mak, *Transplant. Rep.*, 2020, **5**, article no. 100068.

[112] E. A. Ross, *Am. J. Nephrol.*, 2011, **34**, 460-467.

[113] G. Munavalli, A. Reisenauer, M. Moses, S. Kilroy, J. L. Arbiser, *J. Dermatol.*, 2003, **30**, 915-919.

[114] L. Amuluru, W. High, K. M. Hiatt, J. Ranvill, S. V. Shah, B. Malik, S. Swaminathan, *J. Am. Acad. Dermatol.*, 2009, **61**, 73-79.

[115] W. T. Longcope, *J. Am. Med. Assoc.*, 1941, **117**, 1321-1327.

[116] N. Danbolt, *Postgrad. Med. J.*, 1958, **34**, 245-247.

[117] ATS Board of Directors and ERS Executive Committee, "Statement on Sarcoidosis. Joint statement of the American Thoracic Society (ATS), the European Respiratory Society (ERS) and the World Association of Sarcoidosis and Other Granulomatous Disorders (WASOG)", *Am. J. Respir. Crit. Care Med.*, 1999, **160**, no. 2, 736-755.

[118] E. A. Bresnitz, B. L. Strom, *Epidemiol. Rev.*, 1983, **5**, 124-156.

[119] L. S. Newman, C. S. Rose, L. A. Maier, *N. Engl. J. Med.*, 1997, **336**, 1224-1234.

[120] M. A. Hilal, J. Krotva, L. Chichierchio, N. Obeidat, M. Madanat, *G. Ital. Dermatol. Venereol.*, 2010, **145**, 733-745.

[121] A. Lyons, G. Brayman, S. Tahhan, *J. Gen. Intern. Med.*, 2018, **33**, 128-129.

[122] S. M. Ali, A. C. Gilliam, R. T. Brodell, *J. Cutan. Med. Surg.*, 2008, **12**, 43-48.

[123] S. Zhao, Q. Wang, B. Cheng, X.-F. Zhu, *Exp. Ther. Med.*, 2017, **13**, 1535-1537.

[124] J. Müller-Quernheim, M. Schürmann, S. Hofmann, K. I. Gaede, A. Fischer, A. Prasse, G. Zissel, S. Schreiber, *Clin. Chest Med.*, 2008, **29**, 391-414.

[125] J. L. Berlin, G. P. Shantha, H. Yeager, L. Thomas-Hemak, *BMJ Case Rep.*, 2014, **2014**, 1-4.

[126] R. P. Baughman, A. S. Teirstein, M. A. Judson, M. D. Rossman, H. Yeager Jr., E. A. Bresnitz, L. DePalo, G. Hunninghake, M. C. Iannuzzi, C. J. Johns, G. McLennan, D. R. Moller, L. S. Newman, D. L. Rabin, C. Rose, B. Rybicki, S. E. Weinberger, M. L. Terrin, G. L. Knatterud, R. Cherniak, *Am. J. Respir. Crit. Care Med.*, 2001, **164**, 1885-1889.

[127] K. A. Wanat, M. Rosenbach, *Clin. Chest Med.*, 2015, **36**, 685-702.

[128] J. P. Callen, *Arch. Dermatol.*, 2001, **137**, 485-486.

[129] J. Marcoval, A. Moreno, J. Mana, *J. Cutan. Pathol.*, 2004, **31**, 516-517.

[130] N. M. Walsh, J. G. Hanly, R. Tremaine, S. Murray, *Am. J. Dermatopathol.*, 1993, **15**, 203-207.

[131] Y. C. Kim, M. K. Triffet, L. E. Gibson, *Am. J. Dermatopathol.*, 2000, **22**, 408-412.

[132] G. Takemura, Y. Takatsu, K. Ono, T. Miyatake, M. Ono, T. Izumi, H. Fujiwara, *Heart Vessels*, 1995, **10**, 275-278.

[133] Y. Kuribayashi, K. Ohtani, T. Saito, T. Ide, *Eur. Heart J. Cardiovasc. Imaging*, 2017, **18**, 944-945.

[134] M. Catinon, C. Chemarin, F. Thivolet, M. Kambouchner, J.-F.

Bernaudin, C. Cavalin, A.-M. Sfarghiu, F. Arbib, O. Freynet, N. Freymond, J.-F. Mornex, P.-A. Rosental, M. Vincent, D. Valeyre, Ch. Pison, *Eur. Respir. J.*, 2017, **50**, article no. PA3263.

[135] H. Colboc, D. Bazin, Ph. Moguelet, V. Frochot, R. Weil, E. Letavernier, Ch. Jouanneau, C. Frances, C. Bachmeyer, J.-F. Bernaudin, M. Daudon, *C. R. Chim.*, 2016, **19**, 1631-1641.

[136] H. Colboc, P. Moguelet, D. Bazin, C. Bachmeyer, V. Frochot, R. Weil, E. Letavernier, C. Jouanneau, M. Daudon, J. F. Bernaudin, *J. Eur. Acad. Dermatol. Venereol.*, 2019, **33**, 198-203.

[137] L. M. Miller, P. Dumas, *Biochim. Biophys. Acta*, 2006, **1758**, 846-857.

[138] A. Dessombz, D. Bazin, P. Dumas, C. Sandt, J. Sule-Suso, M. Daudon, *PLoS One*, 2011, **6**, article no. e28007.

[139] D. Bazin, E. Letavernier, J.-Ph. Haymann, F. Tielens, A. Kellum, M. Daudon, *C. R. Chim.*, 2016, **19**, 1548-1557.

[140] W. Herschel, J. L. E. Dreyer, *The Scientific Papers of Sir William*, Herschel, Royal Society and Royal Astronomical Society, London, 1912.

[141] J. Chamberlain, *The Principles of Interferometric Spectroscopy*, Wiley, Chichester, UK, 1979.

[142] P. R. Griffiths, J. A. Haseth, *F.T.-IR Spectroscopy in Chemical Analysis: A Series of Monographs on Analytical Chemistry and its Applications*, Wiley, New York, 1986, 38 pages.

[143] D. C. Fernandez, R. Bhargava, S. M. Hewitt, I. W. Levin, *Nat. Biotechnol.*, 2005, **23**, 469-474.

[144] K. C. Khulbe, T. Matsuura, *Polymer*, 2000, **41**, 1917-1935.

[145] C. Krafft, D. Codrich, G. Pelizzo, V. Sergo, *J. Biophoton.*, 2008, **1**, 154-169.

[146] O. P. Sharma, *Curr. Opin. Pulm. Med.*, 2000, **6**, 442-447.

[147] M. Conron, C. Young, H. L. C. Beynon, *Rheumatology*, 2000, **39**, 707-713.

[148] G. W. Hunninghake, U. Costabel, M. Ando, R. Baughman, J. F. Cordier, R. du Bois, A. Eklund, M. Kitaichi, J. Lynch, G. Rizzato, C. Rose, O. Selroos, G. Semenzato, O. P. Sharma, *Sarcoidosis Vasc. Diffuse Lung Dis.*, 1999, **16**, 149-173.

[149] C. E. Broos, M. Van Nimwegen, H. C. Hoogsteden, R. W. Hendriks, M. Kool, B. van den Blink, *Front Immunol.*, 2013, **4**, article no. 437.

[150] A. Deter-Wolf, B. Robitaille, L. Krutak, S. Galliot, *J. Archaeol. Sci. Rep.*, 2016, **5**, 19-24.

[151] N. Kluger, S. Seité, C. Taieb, *J. Eur. Acad. Dermatol. Venereol.*, 2019, **33**, e484-e486.

[152] N. Kluger, L. Misery, S. Seité, C. Taieb, *J. Am. Acad. Dermatol.*, 2019, **81**, 607-610.

[153] G. Prior, *Curr. Probl. Dermatol. Basel, Karger*, 2015, **48**, 152-157.

[154] G. Prior, *Tattoo Inks: Analysis, Pigments, Legislation*, epubli, Berlin, 2014.

[155] M. Manso, S. Pessanha, M. Guerra, U. Reinholz, C. Afonso, M. Radtke, H. Lourenço, M. L. Carvalho, A. G. Buzanich, *Biol. Trace Elem. Res.*, 2019, **187**, 596-601.

[156] H. Petersen, D. Lewe, *Curr. Probl. Dermatol.*, 2015, **48**, 136-141.

[157] A. L. Timko, C. H. Miller, F. B. Johnson, E. Ross, *Arch Dermatol.*, 2001, **137**, 143-147.

[158] S. Gaudron, M.-C. Ferrier-Le Bouëdec, F. Franck, M. D'Incan, *Contact Derm.*, 2014, **72**, 97-105.

[159] J. Serup, K. Hutton Carlsen, N. Dommershausen, M. Sepehri, B. Hesse, C. Seim, A. Luch, I. Schreiver, *Contact Dermatitis*, 2020, **82**, 73-82.

[160] I. Schreiver, C. Hutzler, S. Andree, P. Laux, A. Luch, *Arch. Toxicol.*, 2016, **90**, 1639-1650.

[161] P. Piccinini, S. Pakalin, L. Contor, I. Bianchi, C. Senaldi, 2016, Final Report, EUR27947.

[162] C. of Europe Strasbourg, "Europe C of. Resolution ResAP (2008) 1 on requirements and criteria for the safety of tattoos and permanent make-up (superseding Resolution ResAP (2003) 2 on tattoos and permanent make-up): adopted by the Committee of Ministers on 20 February 2008 at the 1018th meeting of The Ministers' Deputies", 2008.

[163] P. Laux, T. Tralau, J. Tentschert, A. Blume, S. Al Dahouk, W. Bäumler, E. Bernstein, B. Bocca, A. Alimonti, H. Colebrook, Ch. de Cuyper, L. Dähne, U. Hauri, P. C. Howard, P. Janssen, L. Katz, B. Klitzman, N. Kluger, L. Krutak, Th. Platzek, V. Scott-Lang, J. Serup, W. Teubner, I. Schreiver, E. Wilkniß, A. Luch, *Lancet*, 2016, **387**, 395-402.

[164] M. Arl, D. J. Nogueira, J. Schveitzer Köerich, N. Mottim Justino, D. Schulz Vicentini, W. Gerson Matias, *J. Hazard Mater.*, 2019, **364**, 548-561.

[165] E. Maxim, H. Higgins, L. D'Souza, *Int. J. Womens Dermatol.*, 2017, **3**, 228-230.

[166] N. Kluger, D. Douvin, F. Dupuis-Fourdan, J. M. Doumecq-Lacoste, V. Descamps, *Ann. Dermatol. Venereol.*, 2017, **144**, 776-783.

[167] N. Kluger, V. Koljonen, *Lancet Oncol.*, 2012, **13**, e161-e168.

[168] N. Kluger, D. Douvin, F. Dupuis-Fourdan, J.-M. Doumecq-Lacoste, V. Descamps, *Ann. Dermatol. Vénéréol.*, 2017, **144**, 776-783.

[169] H. Colboc, D. Bazin, P. Moguelet, S. Reguer, R. Amode, C. Jouanneau, I. Lucas, L. Deschamps, V. Descamps, N. Kluger, *J. Eur. Acad. Dermatol. Venereol.*, 2020, **34**, e313-e315.

[170] N. C. Scherrer, Z. Stefan, D. Francoise, F. Annette, K. Renate, *Spectrochim. Acta A Mol. Biomol. Spectrosc.*, 2009, **73**, 505-524.

[171] K. H. Carlsen, M. Køcks, M. Sepehri, J. Serup, *Skin Res. Technol.*, 2016, **22**, 460-469.

[172] M. E. Darvin, J. Schleusener, F. Parenz, O. Seidel, C. Krafft, J. Popp, J. Lademann, *Analyst*, 2018, **143**, 4990-4999.

[173] S. L. Schneider, I. Kohli, I. H. Hamzavi, M. L. Council, A. M. Rossi, D. M. Ozog, *J. Am. Acad. Dermatol.*, 2019, **80**, 1121-1131.

[174] D. Bersani, P. P. Lottici, A. Montenero, *J. Raman Spectrosc.*, 1999, **30**, 355-360.

[175] I. Chourpa, L. Douziech-Eyrolles, L. Ngaboni-Okassa, J.-F. Fouquenet, S. Cohen-Jonathan, M. Soucé, H. Marchais, P. Dubois, *Analyst*, 2005, **130**, 1395-1403.

[176] I. Schreiver, B. Hesse, Ch. Seim, H. Castillo-Michel, J. Villanova, P. Laux, N. Dreiack, R. Penning, R. Tucoulou, M. Cotte, A. Luch, *Sci. Rep.*, 2017, **7**, article no. 11395.

[177] I. Schreiver, B. Hesse, Ch. Seim, H. Castillo-Michel, L. Anklamm, J. Villanova, N. Dreiack, A. Lagrange, R. Penning, Ch. De Cuyper, R. Tucoulou, W. Bäumler, M. Cotte, A. Luch, *Part. Fibre Toxicol.*, 2019, **16**, article no. 33.

[178] A. Bianconi, A. Congiu-Castellano, M. Dell'Ariccia, A. Giovannelli, P. J. Durham, E. Burattini, M. Barteri, *FEBS Lett.*, 1984, **178**, 165-170.

[179] *The MAK Collection for Occupational Health and Safety*, vol. 1, Wiley-VCH, Verlag GmbH & Co. KGaA, 2016.

[180] P. S. Islam, Ch. Chang, C. Selmi, E. Generali, A. Huntley, S. S. Teuber, M. E. Gershwin, *Clin. Rev. Allergy Immunol.*, 2016, **50**, 273-286.

[181] T. Høgsberg, K. Loeschner, D. Löf, J. Serup, *Br. J. Dermatol.*, 2011, **165**, 1210-1218.

[182] K. T. Tan, A. G. Messenger, *Br. J. Dermatol.*, 2009, **160**, 75-79.

[183] A. Debroy Kidambi, K. Dobson, S. Holmes, D. Carauna, V. Del Marmol, A. Vujovic, M. R. Kaur, A. Takwale, P. Farrant, C. Champagne, M. Harries, A. G. Messenger, *Br. J. Dermatol.*, 2017, **177**, 260-261.

[184] J. Lademann, H. Weigmann, C. Rickmeyer, H. Barthelmes, H. Schaefer, G. Mueller, W. Sterry, *Skin Pharmacol. Appl. Skin Physiol.*, 1999, **12**, 247-256.

[185] A. Somogyi, K. Medjoubi, G. Baranton, V. Le Roux, M. Ribbens, F. Polack, P. Philippot, J. P. Samama, *J. Synchrotron Radiat.*, 2015, **22**, 1118-1129.

[186] E. Esteve, D. Bazin, Ch. Jouanneau, S. Rouzière, A. Bataille, A. Kellum, K. Provost, Ch. Mocuta, S. Reguer, D. Thiaudiere, K. Jorissen, J. J. Rehr, A. Hertig, E. Rondeau, E. Letavernier, M. Daudon, P. Ronco, *C. R. Chim.*, 2016, **19**, 1580-1585.

[187] E. Esteve, D. Bazin, Ch. Jouanneau, S. Rouzière, A. Bataille, A. Kellum, K. Provost, Ch. Mocuta, S. Reguer, D. Thiaudiere, K. Jorissen, J. J. Rehr, A. Hertig, E. Rondeau, E. Letavernier, M. Daudon, P. Ronco, *C. R. Chim.*, 2016, **19**, 1586-1589.

[188] E. Esteve, S. Reguer, C. Boissiere, C. Chanéac, G. Lugo, Ch. Jouanneau, C. Mocuta, D. Thiaudière, N. Leclercq, B. Leyh, J.-F. Greisch, J. Berthault, M. Daudon, P. Ronco, D. Bazin, *J. Synchrotron Radiat.*, 2017, **24**, 991-999.

[189] T. Inoue, K. Takehara, N. Shimizu, Y. Kitajima, K. Shinohara, A. Ito, *J. X-ray Sci. Technol.*, 2011, **19**, 313-320.

[190] C. Couteau, H. Diarra, Z. Schmitt, L. Coiffard, *Eur. J. Dermatol.*, 2019, **29**, 141-159.

[191] J. Siritapetawee, W. Pattanasiriwisawa, U. Sirithepthawee, *J. Synchrotron Radiat.*, 2010, **17**, 268-272.

[192] A. Bertazzo, C. Costa, M. Biasiolo, G. Allegri, G. Cirrincione, G. Presti, *Biol. Trace Element Res.*, 1996, **52**, 37-53.

[193] L. Dastgheib, Z. Mostafavi-pour, A. A. Abdorazagh, Z. Khoshdel, M. S. Sadati, I. Ahrari, S. Ahrari, M. Ghavipisheh, *Dermatol. Res. Pract.*, 2014, **2014**, article no. 784863.

[194] G. Ozaydin-Yavuz, I. Halil Yavuz, H. Demir, C. Demir, S. G. Bilgili, *Indian J. Dermatol.*, 2019, **64**, 7-11.

[195] I. Nicolis, P. Deschamps, E. Curis, P. Chevallier, O. Corriol, V. Colomb, S. Bénazeth, *J. Trace Microprobe Techn.*, 2000, **18**, 511-516, Informa UK (Marcel Dekker).

[196] E. Y. Bonnist, P. D. Pudney, L. A. Weddell, J. Campbell, F. L. Baines, S. E. Paterson, J. R. Matheson, *Int. J. Cosmet. Sci.*, 2014, **36**, 347-354.

[197] K. Müller, E. Valentine-Thon, *Neuro Endocrinol. Lett.*, 2006, **27**, 31-35.

[198] S. G. Han, B. Newsome, B. Hennig, *Toxicology*, 2013, **306**, 1-8.

[199] T. Wu, M. Tang, *Nanomedicine (Lond)*., 2018, **13**, 233-249.

[200] P. J. Caspers, G. W. Lucassen, R. Wolthuis, H. A. Bruining, G. J. Puppels, *Biospectroscopy*, 1998, **4**, S31-S39.

[201] H. Lui, J. Zhao, D. McLean, H. Zeng, *Cancer Res.*, 2012, **72**, 2491-2500.

[202] C. A. Lieber, S. K. Majumder, D. L. Ellis, D. D. Billheimer, A. Mahadevan-Jansen, *Lasers Surg. Med.*, 2008, **40**, 461-467.

[203] P. J. Caspers, G. W. Lucassen, G. J. Puppels, *Biophys. J.*, 2003, **85**, 572-580.

[204] A. P. M. Michel, S. Liakat, K. Bors, C. F. Gmach, *Biomed. Opt. Express*, 2013, **4**, 520-530.

[205] A. Bauer, O. Hertzberg, A. Küderle, D. Strobel, M. A. Pleitez, W. Mäntele, *J. Biophoton.*, 2018, **11**, article no. e201600261.

[206] D. A. Bradley, M. J. Farquharson, *J. Radioanal. Nucl. Chem.*, 2000, **244**, 213-217.

[207] H. Shehab, E. D. Desouza, J. O'Meara, A. Pejović-Milić, D. R. Chettle, D. E. B. Fleming, F. E. McNeill, *Physiol. Meas.*, 2016, **37**, 145-161.

[208] F. Fercher, *J. Biomed. Opt.*, 1996, **1**, 157-173.

[209] Gh. Podoleanu, *J. Microsc.*, 2012, **247**, 209-219.

[210] M. Zysk, F. T. Nguyen, A. L. Oldenburg, D. L. Marks, S. A. Boppart, *J. Biomed. Opt.*, 2007, **12**, article no. 051403.

[211] J. S. Schuman, C. A. Puliafito, J. G. Fujimoto, J. S. Duker, *Optical Coherence Tomography of Ocular Diseases*, 3rd ed., Slack Inc., Thorofare, NJ, 2013.

[212] H. G. Bezerra, M. A. Costa, G. Guagliumi, A. M. Rollins, D. I. Simon, *JACC Cardiovasc. Interv.*, 2009, **2**, 1035-1046.

[213] D. C. Adler, Y. Chen, R. Huber, J. Schmitt, J. Connolly, J. G. Fujimoto, *Nat. Photon.*, 2007, **1**, 709-716.

[214] X. Yu, Q. Ding, C. Hu, G. Mu, Y. Deng, Y. Luo, Z. Yuan, H. Yu, L. Liu, *IEEE J. Sel. Top. Quantum Electron*, 2019, **25**, 1-8.

[215] J. Men, Y. Huang, J. Solanki, X. Zeng, A. Alex, J. Jerwick, Z. Zhan, R. E. Tanzi, A. Li, C. Zhou, *IEEE J. Sel. Top. Quantum Electron*, 2016, **22**, article no. 6803213.

[216] Y. Fan, Y. Xia, X. Zhang, Y. Sun, J. Tang, L. Zhang, H. Liao, *Biosci. Trends*, 2018, **18**, 12-23.

[217] A. Levine, K. Wang, O. Markowitz, *Dermatol. Clin.*, 2017, **35**, 465-488.

[218] A. Dubois, O. Levecq, H. Azimani, D. Siret, A. Barut, M. Suppa, V. Del Marmol, J. Malvehy, E. Cinotti, J. L. Perrot, *J. Biomed. Opt.*, 2018, **23**, article no. 106007.

[219] G. Pothier Bouchard, S. M. Mentzer, J. Riel-Salvatore, J. Hodgkins, Ch. E. Miller, F. Negrino, R. Wogelius, M. Buckley, *J. Archaeol. Sci. Rep.*, 2019, **26**, article no. 101862.

[220] S. Bertazzo, E. Gentleman, *Eur. Heart J.*, 2017, **38**, 1189-1193.

[221] J. D. Hutcheson, C. Goettsch, S. Bertazzo, N. Maldonado, J. L. Ruiz, W. Goh, K. Yabusaki, T. Faits, C. Bouten, G. Franck, Th. Quillard, P. Libby, M. Aikawa, S. Weinbaum, E. Aikawa, *Nat. Mater.*, 2016, **15**, 335-343.

[222] C. Verrier, D. Bazin, L. Huguet, O. Stéphan, A. Gloter, M.-Ch. Verpont, V. Frochot, J.-Ph. Haymann, I. Brocheriou, O. Traxer, M. Daudon, E. Letavernier, *J. Urol.*, 2016, **196**, 1566-1574.

[223] M. A. Aronova, R. D. Leapman, *MRS Bull.*, 2012, **37**, 53-62.

[224] C. Gay, E. Letavernier, M.-Ch. Verpont, M. Walls, D. Bazin, M. Daudon, N. Nassif, O. Stephan, M. de Frutos, *ACS Nano.*, 2020, **14**, 1823-1836.

[225] A. Dazzi, F. Glotin, R. Carminati, *J. Appl. Phys.*, 2010, **107**, article no. 124519.

[226] A. Dazzi, C. B. Prater, *Chem. Rev.*, 2017, **17**, 5146-5173.

[227] E. Esteve, Y. Luque, J. Waeytens, D. Bazin, L. Mesnard, Ch. Jouanneau, P. Ronco, A. Dazzi, M. Daudon, A. Deniset-Besseau, *Anal. Chem.*, 2020, **92**, 7388-7392.

[228] D. Bazin, M. Rabant, J. Mathurin, M. Petay, A. Deniset-Besseau, A. Dazzi, Y. Su, E. P. Hessou, F. Tielens, F. Borondics,

M. Livrozet, E. Boudelicque, J.-Ph. Haymann, E. Letavernier, V. Frochot, M. Daudon, *C. R. Chim.*, 2022, **25**, no. S1, 489-502.

[229] F. Jamme, S. Villette, A. Giuliani, V. Rouam, F. Wien, B. Lagarde, M. Réfrégiers, *Microsc. Microanal.*, 2010, **16**, 507-514.

[230] E. Batard, F. Jamme, S. Villette, C. Jacqueline, M.-F. de la Cochetière, J. Caillon, M. Réfrégiers, *PLoS One*, 2011, **6**, article no. 19440.

[231] F. Jamme, S. Kascakova, S. Villette, F. Allouche, S. Pallu, V. Rouam, M. Réfrégiers, *Biol. Cell*, 2013, **105**, 277-288.

[232] M. Strupler, M. Hernest, C. Fligny, J.-L. Martin, P.-L. Tharaux, M.-C. Schanne-Klein, *J. Biomed. Opt.*, 2008, **13**, article no. 054041.

[233] N. Vuillemin, P. Mahou, D. Débarre, Th. Gacoin, P.-L. Tharaux, M.-C. Schanne-Klein, W. Supatto, E. Beaurepaire, *Sci. Rep.*, 2016, **6**, article no. 29863.

[234] A.-M. Pena, Th. Boulesteix, Th. Dartigalongue, M.-C. Schanne-Klein, *J. Am. Chem. Soc.*, 2005, **127**, 10314-10322.

[235] K. Benzerara, F. Skouri-Panet, J. Li, C. Férard, M. Gugger, Th. Laurent, E. Couradeau, M. Ragon, J. Cosmidis, N. Menguy, I. Margaret-Oliver, R. Taver, P. López-Garcíac, D. Moreira, *Proc. Natl. Acad. Sci. USA*, 2014, **111**, 10933-10938.

[236] P. Hohenberg, W. Kohn, *Phys. Rev. B*, 1964, **136**, 864-871.

[237] R. O. Jones, *Rev. Mod. Phys.*, 2015, **87**, 897-923.

[238] N. Mardirossian, M. Head-Gordon, *Mol. Phys.*, 2017, **115**, 2315-2372.

[239] M. Cutini, M. Corno, D. Costa, P. Ugliengo, *J. Phys. Chem. C*, 2019, **123**, 7540-7550.

[240] M. Corno, C. Busco, V. Bolis, S. Tosoni, P. Ugliengo, *Langmuir*, 2009, **25**, 2188-2198.

[241] A. Rimola, M. Aschi, R. Orlando, P. Ugliengo, *J. Am. Chem. Soc.*, 2012, **134**, 10899-10910.

[242] D. Bazin, F. Tielens, *Appl. Catal.*, 2015, **504**, 631-641.

[243] F. Tielens, D. Bazin, *C. R. Chim.*, 2018, **21**, 174-181.

[244] I. C. Oğuz, H. Guesmi, D. Bazin, F. Tielens, *J. Phys. Chem. C*, 2019, **123**, 20314-20318.